Black Holes and Trapped Surfaces

Emma Jakobsson

Licentiate Thesis in Theoretical Physics

Akademisk avhandling för avläggande av licentiatexamen vid Stockholms universitet, Fysikum

June 2014

Stockholms universitet

Abstract

The study of black holes is an important part of general relativity. However, the very definition of black holes is not completely satisfactory. Alternative definitions are based on the concept of trapped surfaces. This licentiate thesis is based on work with the aim to better understand the behaviour of such trapped surfaces.

The standard definition of a black hole and specific examples are reviewed, as well as the definition of trapped surfaces, various horizons related to trapped surfaces, and the trapping boundary. This serves as an introduction to two published papers. The first paper provides an exact model of a marginally trapped tube making a sudden jump outwards as matter is falling into the black hole. The second paper concerns the question of the location of the trapping boundary in the Oppenheimer-Snyder black hole.

Acknowledgements

First of all I would like to thank my supervisor Ingemar Bengtsson for being an excellent guide and source of inspiration. Secondly, I would like to thank José M. M. Senovilla for a fruitful collaboration, and for getting the opportunity to visit Bilbao.

A big thankyou to my room mates Sören Holst and Thomas Kvorning for (mostly) entertaining conversations, making the work hours most enjoyable. I would also like to thank my partner Jonas for his endless support, and for providing me with food. Finally, thank you to the rest of the condensed matter group for creating a friendly work environment.

Contents

List of accompanying papers

Paper I	**How trapped surfaces jump in 2+1 dimensions** E. Jakobsson *Class. Quant. Grav.* **30** (2013) 065022 (arXiv:1208.6160 [gr-qc])
Paper II	**Trapped surfaces in Oppenheimer-Snyder black holes** I. Bengtsson, E. Jakobsson, and J. M. M. Senovilla *Phys. Rev.* **D88** (2013) 064012 (arXiv:1306.6486 [gr-qc])

Chapter 1

Introduction

1.1 Black holes

General relativity is a theory of gravity. Einstein's insight was that the attractive force between massive objects—as in Newtonian mechanics—should not be viewed as a force at all, but rather as a spacetime curvature. Thus the theory of gravity became a geometrical theory.

The theory of general relativity is summarized in Einstein's equations. They are a set of non-linear second order partial differential equations, whose solutions describe the relation between the geometry and the matter distribution of spacetime. This statement should not be misunderstood. It does not mean that the spacetime geometry is solved for given an initial matter distribution; a distribution of matter has no meaning without a spacetime to be distributed in. The dynamics of space and matter are intertwined and must be solved for simultaneously, making it difficult to find solutions to Einstein's equations. Here we will consider solutions with the four dimensions we are accustomed to in our everyday life: three spatial dimensions and one time dimension. One way to go about the problem is to ask the computer for help with massive simulations, as is done in the field of numerical relativity (see for example [1]). When it comes to exact, global solutions of physical interest, there are not that many known ones to choose from. And furthermore, these often contain singularities. Such singularities are not considered to be part of the spacetime. As a consequence, it may be that some geodesics end in finite parameter time; the spacetime is then *geodesically incomplete*. Singularities can appear in many different forms, and it is desirable to have a general definition of a singularity, applying to all the different varieties. In fact, geodesic incompleteness is the most common definition of a singular spacetime.

The presence of a singularity may give rise to the notion of a *black hole*. A black hole spacetime is divided into interior and exterior regions. The boundary between these two regions is called the *event horison*. Vaguely put: the exterior region is such that timelike and lightlike curves may be extended to infinity. This is obviously not the case for an incomplete geodesic. Thus, the standard definition of a black hole relies on a proper definition of "infinity". This definition can only be applied to spacetimes to which we can add a boundary. With a suitable choice of coordinates it may be possible to multiply the metric by a conformal factor such that infinity is brought to points at finite coordinate values. These points then define a boundary of the spacetime. This boundary is referred to as *conformal infinity*, usually denoted $\mathscr{I}$ [2]. The exterior region may be defined as the *chronological past* of future infinity $\mathscr{I}^+$. That is, the set of points from which a timelike curve may reach future infinity. If all of the spacetime is not included in this set, there is a black hole, and an event horizon may be defined as the boundary of the exterior region. Note that the presence of a singularity—that is, geodesic incompleteness—alone does not predict a black hole spacetime. It is the existence of an event horizon that defines a black hole. In this thesis we will investigate alternative black hole definitions, not involving boundaries at infinity, and thus applying to a wider range of spacetimes.

We have seen that the whole idea of black holes stems from the emergence of singularities in solutions to Einstein's equations. But even though a quantum theory of gravity might resolve the problem of singularities, the fact that there are black holes out there is generally accepted and undisputed. This is due to observations made by astronomers, that are most easily explained by the presence of black holes. Such observations indicate that there are large black holes at the centre of many galaxies, including our own.

1.2 Outline

In Chapter 2 some examples of black hole solutions are described. The Schwarzschild and Reissner-Nordström solutions are basic and important examples of black holes. The Oppenheimer-Snyder solution is a fairly realistic model of a spherical star undergoing gravitational collapse. It forms the basis for the work of Paper II.

In Chapter 3 the definition and meaning of trapped surfaces is reviewed. Both Paper I and II are concerned with trapped surfaces, and Chapter 3 gives a motivation for this line of work. Some important concepts related to trapped surfaces are explained, and certain properties of trapped surfaces are investigated.

Together, Chapter 2 and 3 provide an introduction to Paper I and II. A complementary background to Paper I is given in [3].

Chapter 2

Black hole solutions

2.1 Schwarzschild

The first black hole solution was found by Schwarzschild [4], only a few months after Einstein published his vacuum equations [5]. The Schwarzschild spacetime is intended to describe the gravitational field outside a static and perfectly spherical body, e.g. a star, and does so perfectly well. It was first understood to also be a black hole solution in 1958 [6].

In a spherically symmetric spacetime, there are preferred round 2-spheres that are invariant under rotations. An *area radius* r can be defined through the area A of each such sphere, as $A = 4\pi r^2$. Using r as a coordinate, the general form of a spherically symmetric and static metric is

$$ds^2 = -V(r)dt^2 + \frac{dr^2}{V(r)} + r^2(d\theta^2 + \sin^2\theta d\phi^2), \tag{2.1}$$

where t is a time coordinate, and θ, ϕ are the spherical coordinates of the 2-spheres. The above metric solves Einstein's vacuum equations if

$$V(r) = 1 - \frac{2M}{r}. \tag{2.2}$$

Note that as r grows large, the metric (2.1) approaches the flat metric; the Schwarzschild solution is *asymptotically flat*. Since gravity is described by curvature, the model is that of an isolated body, far from which the gravitational field tends to zero. This is a reasonable approximation of a real physical situation, considering the great distances between heavy objects such as stars in our universe. The constant M corresponds to the mass of the body in the Newtonian limit.

At $r = 2M$ the Schwarzschild metric breaks down. However, this is nothing more than a coordinate singularity. With a suitable choice of coordinates, the Schwarzschild solution can be extended beyond this peculiar hypersurface [7]. But at $r = 0$ there is a true singularity, where the curvature

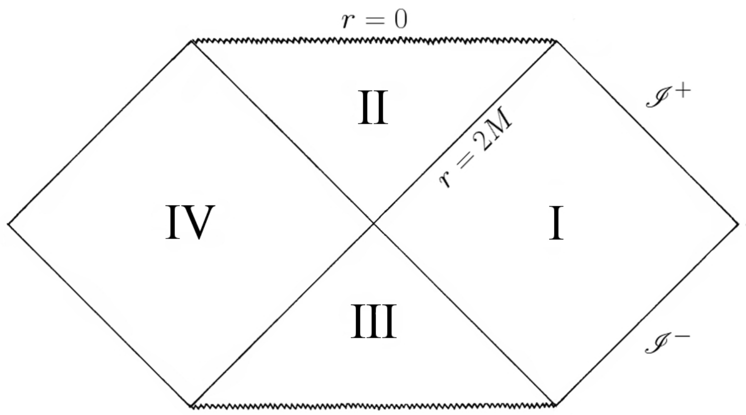

Figure 2.1: A Penrose diagram of the Schwarzschild black hole. $\mathscr{I}^+$ refers to future conformal infinity, and $\mathscr{I}^-$ to past conformal infinity.

of spacetime becomes infinite. The null surface $r = 2M$ is the event horizon of a black hole.

Note that inside the event horizon, r becomes a timelike coordinate, while t becomes spacelike. This is the region inside the black hole, and the gravitational field has become so strong that even light can not escape. Here the future inevitably means that r decreases, until the singularity at $r = 0$ is reached; thus r becomes a time coordinate.

One way to get an overview of a spherically symmetric spacetime is to draw a *Penrose diagram* [8]. We make use of the symmetry and let each 2-sphere be represented by a point, in order to obtain a two dimensional diagram. With a suitable choice of coordinates we may draw a conformally compactified picture of the whole spacetime, including infinity. Furthermore, in 1+1 dimensions it is always possible to choose coordinates such that null geodesics are depicted as straight lines. Conveniently, null geodesics are conformally invariant, and are thus left untouched by the conformal compactification. By convention, the conformal compactification is done in a way such that these straight lines—representing radial null geodesics—have a slope of 45°. Thus the causal structure of the spacetime becomes clear.

The Penrose diagram of the extended Schwarzschild spacetime is shown in Fig 2.1. There are four regions depicted in this diagram. Region I is the exterior region where $r > 2M$. Region II, containing the singularity at $r = 0$, lies at $r < 2M$, inside the black hole. Region III also contains a singularity in the far past, and is often referred to as a "white hole". Region IV is another asymptotic region, identical to and causally disconnected from region I.

If the solution is to describe a physical object with a reasonable history, region III and IV are regarded as unphysical. Then, the Schwarzschild solution describes the *exterior* of a massive body, and is only valid down to the radius of this spherical object. If the radius of the object is larger than twice its mass, there is nothing peculiar going on; we are looking at an object such as a star, and only region I of the Penrose diagram is relevant. In a situation where the radius of the body becomes less than $2M$, it undergoes *gravitational collapse*, and a black hole is formed. In this situation, region II is also relevant.

We will come back to the Schwarzschild solution in Section 2.3, where a model of an interior of a star is matched with the exterior Schwarzschild solution.

2.2 Reissner-Nordström

The Reissner-Nordström solution describes a black hole with mass and *electric charge*. It was discovered shortly after the Schwarzschild solution [9, 10]. Again, we consider a static and spherically symmetric solution, with metric (2.1). But this time an electromagnetic field will be present in the spacetime. Einstein's equations for an electromagnetic field in vacuum are called the *Einstein-Maxwell equations*. These are solved with

$$V(r) = 1 - \frac{2M}{r} + \frac{e^2}{r^2}, \tag{2.3}$$

where the parameter e is a measure of electric charge, appearing in the solution for the electromagnetic field. We have a black hole solution if $e < M$. Then there are coordinate singularities at

$$r_{\pm} = m \pm \sqrt{m^2 - e^2}. \tag{2.4}$$

There will now be two horizons: an outer horizon at r_+, and an inner horizon at r_-. The outer horizon is the event horizon of the black hole, and the inner horizon is a so called *Cauchy horizon*; whatever happens beyond the Cauchy horizon could never be predicted from the evolution of an initial data hypersurface. But—as in the Schwarzschild case—the Reissner-Nordström solution can be extended beyond the horizons [11] and, again, there will be a true singularity at $r = 0$.

The Penrose diagram of the extended Reissner-Nordström black hole is in some regards similar to, but in others quite different from, that of the Schwarzschild solution, see Fig 2.2. Again, there are two causally disconnected asymptotic regions (I and IV), and the spacetime is asymptotically flat. There is a white hole in region III. Beyond the event horizon at r_+, there is an interior region II. This region is bounded to the future by the inner horizon, and we can extend the diagram further into region V and VI. Here we come across *timelike* singularities at $r = 0$, one in each region. Now, the solution can be extended even further into a region VII, identical in structure

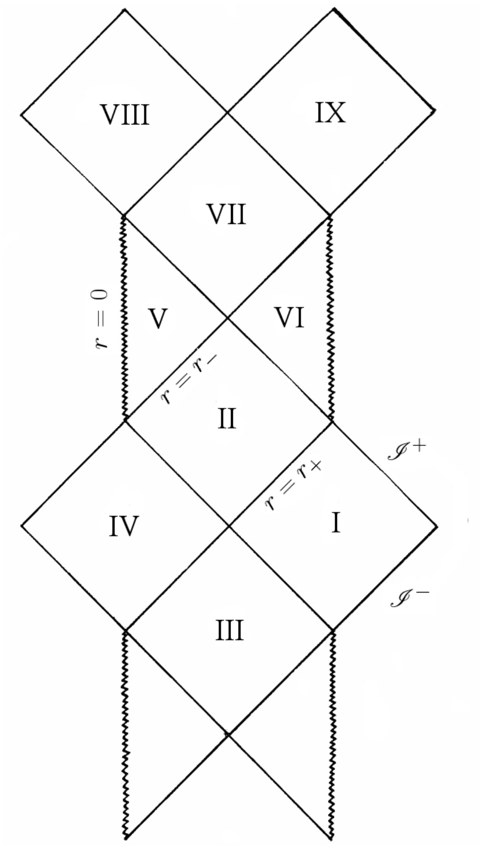

Figure 2.2: A Penrose diagram of the Reissner-Nordström black hole.

to region III. And from there we may reach asymptotic regions VIII and IX, identical to regions I and IV. And so on, the solution can be continuously extended to the future, as well as to the past. A freely falling observer would never reach the singularity, but "bounce back" into the next white hole, then reach a new asymptotic region. It seems that the Reissner-Nordström solution is even "more unphysical" than the Schwarzschild solution. Region I perfectly well describes the field surrounding a spherically symmetric and charged body. In the case of gravitational collapse, region II is relevant. It is not clear whether the regions V and VI are relevant or not. The inner horizon, separating these regions from region II, possesses instability properties. It could be that in a physical situation a true singularity will form in its vicinity [12, 13]. If it is so, there would not be a Cauchy horizon; the whole spacetime could be uniquely determined from intial data.

It is worth remarking that also if $e = M$ we have a black hole solution. Then there will only be one horizon at $r = M$. This is a so called *extreme black hole*. It is quite different from the nonextreme Reissner-Nordström black hole. The limiting procedure $e \to M$—as well as the limit $e \to 0$, yielding the Schwarzschild black hole—is quite nontrivial, even though it might not seem so at a first glance. Much more can be said about this, which I intend to do elsewhere [14].

We have now reviewed the static and spherically symmetric Schwarzschild black hole and its generalization, the charged Reissner-Nordström black hole. Further *stationary* generalizations are found in the *Kerr black hole* [15], possessing mass and angular momentum, and the *Kerr-Newman solution* [16], possessing electric charge as well. Details can be found elsewhere [17]. And here the story ends. The Kerr solution is the *unique* stationary vacuum black hole solution; the black hole is uniquely described by its mass and angular momentum. And the charged Kerr-Newman black hole is the unique stationary *electrovac* black hole, determined only by its mass, angular momentum and charge. This is usually referred to as the *no-hair theorem*.

2.3 Oppenheimer-Snyder

As we have seen, the extended Schwarzschild and Reissner-Nordström solutions are partly unphysical. The *Oppenheimer-Snyder solution* attempts to be a physical model of gravitational collapse [18]. Here, the collapsing body is modelled by a spherical cloud of dust, and its exterior is described by the Schwarzschild solution.

The vacuum Schwarzschild solution we already know, but to model the dust cloud we need a solution to Einstein's equations with a matter distribution. The simplest assumptions we can make is that spacetime is homogeneous and isotropic. In general, under these assumptions, space has constant curvature. Considering a space of constant positive curvature—that is, a 3-sphere—, the spacetime metric takes the form

$$ds^2 = -dt^2 + a^2(t)(d\chi^2 + \sin^2 \chi d\Omega^2), \tag{2.5}$$

where $d\Omega^2$ is the metric of a 2-sphere. The expression within brackets is the metric of a 3-sphere, where the coordinate χ runs between 0 and π. The function a—determining the size of the universe at given times—must be solved for depending on the mass distribution considered. Here we consider pressureless dust. Einstein's equations together with the condition for energy conservation then yields a solution on parameter form

$$\begin{aligned} a(\eta) &= \frac{a_m}{2}(1 - \cos\eta), \\ t(\eta) &= \frac{a_m}{2}(\eta - \sin\eta), \end{aligned} \tag{2.6}$$

where a_m is a constant related to the minimum energy density of the dust. The function (2.6) describes a *cycloid*; its graph is obtained by letting a point on a circular wheel draw a curve as the wheel rolls along a straight line.

The above solution is called the *Friedmann model* [19]. This dust-filled universe begins with an initial singularity, when the timelike parameter η takes the value zero. Then it expands until $\eta = \pi$, when it starts shrinking again. At $\eta = 2\pi$ it ends in a final singularity. It is a *closed* universe; it is compact without boundary.

Here we will only consider part of this universe and let it model a spherical cloud of dust. We let the surface of the dust cloud be given by a timelike hypersurface where the coordinate χ takes a constant value $\chi_0 < \pi/2$. It is a hypersurface foliated by round 2-spheres of radius $R(\eta) = a(\eta)\sin\chi_0$ at any given value of η. We are here concerned with the collapsing phase $\eta > \pi$ of the Friedmann model. The surface of the dust cloud is then matched to a timelike hypersurface in the Schwarzschild spacetime on which the area radius $r = R(\eta)$. This matching has to be done properly, satisfying certain conditions on smoothness. Details will not be given here, but may be found in the literature [20]. With a proper matching, the parameters of the Friedmann and Schwarzschild solutions are related by

$$M = \frac{a_m}{2}\sin^3\chi_0. \tag{2.7}$$

A Penrose diagram of the Oppenheimer-Snyder black hole is shown in Fig. 2.3.

The Oppenheimer-Snyder solution is a special case of a more general family of solutions that go by the name of *Tolman-Bondi solutions*. These describe the gravitational collapse of spherically symmetric, in general inhomogeneous, clouds of dust. In the Oppenheimer-Snyder solution, the *cosmic censorship hypothesis* holds. The cosmic censorship hypothesis—which has not been proven, but is generally considered to hold true—states that a singularity is always hidden behind an event horizon; there are no so called naked singularities. This is not always the case in a more general Tolman-Bondi solution [21]. In this regard the Oppenheimer-Snyder solution seems physically realistic. In spite of its simplicity, the Oppenheimer-Snyder model is generally believed to give a reasonable account for what happens when a body undergoes gravitational collapse.

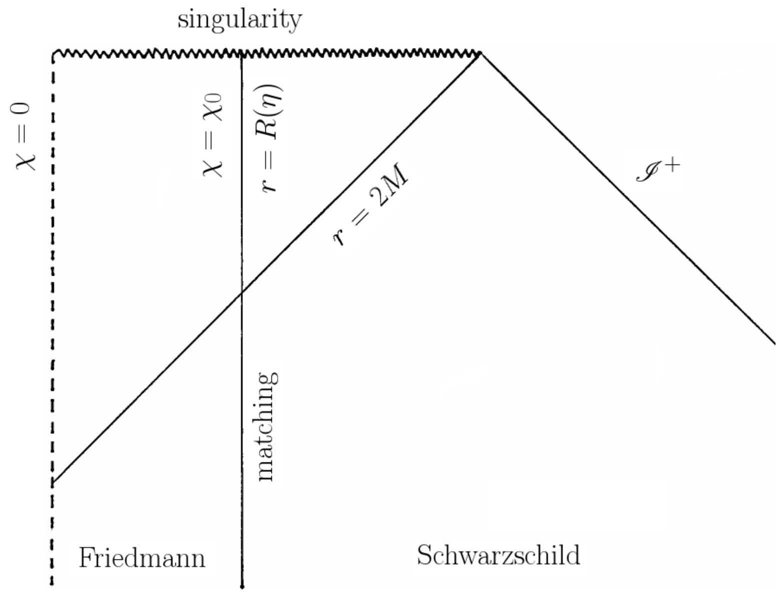

Figure 2.3: A Penrose diagram covering the collapsing phase of the Oppenheimer-Snyder model. The centre of the dust cloud sits at $\chi = 0$, and its surface is at $\chi = \chi_0$. In the exterior the surface is given by $r = R(\eta)$. The vacuum exterior region is represented by the Schwarzschild solution.

Chapter 3

Trapped surfaces

As already stated, a black hole is defined by its event horizon. But the event horizon, as it is defined, could never be *observed* in any way. Only once the infinite future is known, can the location of the event horizon be established. Neither in a real physical situation, nor in a numerical evolution of spacetime, can any event horizon be located exactly. To quote Hayward [22]:

> The event horizon does not have any physical effect. Such a horizon could be passing through you, gentle reader, at any given instant; no-one would notice.

However, there may be hints that a black hole has been formed. In this context *trapped surfaces* [23] become interesting.

3.1 What is a trapped surface?

The surfaces we consider are two-dimensional, spacelike, and closed; in practice, they are topological spheres. A two-dimensional surface in a four-dimensional spacetime has two null directions normal to the surface at each point. Thus we can distinguish two future directed families of null geodesics emerging from the surface. Under normal circumstances—think of the surface as roughly a sphere—one family of light rays will be directed outwards, and the other directed inwards. Here, and in the following, we shall assume that there is a natural notion of an "outer" and an "inner" direction. These notions are quite intuitive in many cases. If both of the families of light rays orthogonal to the surface converge, the surface is said to be trapped. That is, if a flash of light is emitted from every point of the surface simultaneously, the ingoing as well as the outgoing wavefront will decrease in area. To be exact, the above description is that of a *future* trapped surface. These are of interest when considering gravitational collapse. In the context of cosmology, the notion of *past* trapped surfaces becomes interesting. Such surfaces may be defined in a similar manner.

It is quite intuitive that something strange is going on if a trapped surface is present. In a Minkowski spacetime the ingoing wavefront of a closed surface would decrease in area, while the outgoing wavefront would *increase*. That the outgoing family of lightrays converges is a sign of a strong gravitational field, tending to focus the light. Note though that it may be possible to find trapped surfaces in a flat spacetime. By taking a surface being the intersection of two past light cones in Minkowski space, we see that there are surfaces such that the two families of light rays both converge. But these will not be *closed*, and are therefore not trapped by definition. However, such "locally trapped" surfaces may be closed by performing identifications in Minkowski spacetime. The resulting spacetime is called *Misner space* [24], which is a flat spacetime containing trapped surfaces. A similar kind of identification in 2+1-dimensional anti-de Sitter space yields a black hole model [25]. It is a toy model, with one dimension less, and thus the notion of trapped surfaces must be replaced by trapped curves. Trapped curves in such a spacetime are investigated in Paper I.

In order to give the technical definition of a trapped surface, some terminology is needed. The *first fundamental form* is the induced metric on the surface. As such, it contains information about the *intrinsic* curvature of the surface. Suppose that $\{\vec{e}_A\}$, $A = 1, 2$, are tangent vectors spanning the tangent plane at a point on the surface. Then the first fundamental form γ_{AB} at this point is given by

$$\gamma_{AB} = e^a_A e^b_B g_{ab}, \tag{3.1}$$

where g_{ab}, $a, b = 1, ..., 4$, is the full spacetime metric.

Now suppose that $\vec{n}$ is a unit normal vector to the surface at a point. Then the *shape operator* $S_{\vec{n}}$ (also known as the *Weingarten map*) is defined as the directional derivative of $\vec{n}$ along a tangent vector $\vec{t}$ of the surface at that same point:

$$\begin{aligned} S_{\vec{n}}(\vec{t}) &= \nabla_{\vec{t}}\vec{n} \\ &= t^b \nabla_b \vec{n}. \end{aligned} \tag{3.2}$$

The shape operator measures at what rate the normal vector changes as we move along the surface—or, in other words, it measures the *extrinsic* curvature of the surface.

Now we define the bilinear form

$$\begin{aligned} K_{\vec{n}}(\vec{u}, \vec{v}) &= \vec{u} \cdot S_{\vec{n}}(\vec{v}) \\ &= u^a v^b \nabla_b n_a, \end{aligned} \tag{3.3}$$

where the vectors $\vec{u}, \vec{v}$ are tangent to the surface. If the codimension is one, $K_{\vec{n}}$ is known as the *second fundamental form*. Its components in terms of the basis $\{\vec{e}_A\}$ on the tangent plane are

$$\begin{aligned} K_{AB}(\vec{n}) &= e^a_A e^b_B \nabla_b n_a \\ &= -n_a e^b_B \nabla_b e^a_A. \end{aligned} \tag{3.4}$$

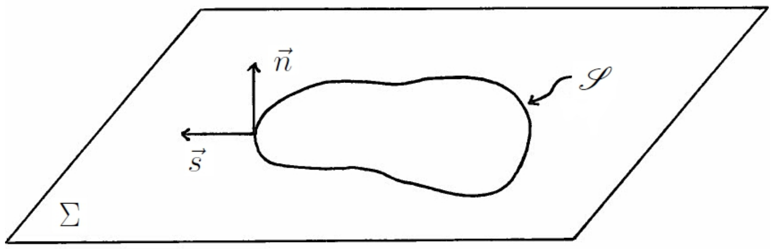

Figure 3.1: A spacelike hypersurface Σ with one dimension suppressed. The closed surface $\mathscr{S}$ lies in Σ. At each point of $\mathscr{S}$ there are two vectors orthogonal to the surface: $\vec{s}$ lying in Σ and $\vec{n}$ orthogonal to Σ.

The reformulation on the second line above—which follows from the fact that $\vec{e}_A$ and $\vec{n}$ are orthogonal—is more convenient for calculations. The expressions (3.1)-(3.4) are properties of the surface under consideration, and are understood to be evaluated *at the surface*.

Now, consider a closed spacelike surface $\mathscr{S}$; let us for simplicity assume that it is a topological sphere. Suppose that there is a three-dimensional spacelike hypersurface Σ containing $\mathscr{S}$, see Fig. 3.1. Then we can identify a spacelike unit normal field $\vec{s}$ lying in the hypersurface, pointing out of the topological sphere $\mathscr{S}$. There will also be a future directed timelike unit normal field $\vec{n}$, orthogonal to Σ. Then we may define an outgoing future directed null normal field $\vec{k}_+$ and an ingoing future directed null normal field $\vec{k}_-$ by

$$\vec{k}_\pm = \vec{n} \pm \vec{s}. \tag{3.5}$$

This fixes the normalization to be

$$\vec{k}_+ \cdot \vec{k}_- = -2. \tag{3.6}$$

The *null expansions* $\theta_\pm$ of the congruences of lightlike geodesics with tangent vector fields $\vec{k}_\pm$ are evaluated as

$$\theta_\pm = \gamma^{AB} K_{AB}(\vec{k}_\pm) \tag{3.7}$$

on the surface $\mathscr{S}$. As the name implies, the null expansions measure to what extent the congruences of light rays expand. If the null expansion is negative, the lightrays do not expand at all, but rather tend to contract. Thus, we have the tools to find out whether a surface is trapped or not, by computing the null expansions θ_+ and θ_- and checking if they are both negative. The actual value of the null expansions depends on the choice of null normals. There is no unique way to choose these; the definition (3.5) given above depends on the choice of the hypersurface Σ. The normalization (3.6) does not determine the null normals uniquely either. We may always introduce

	θ_+	θ_-
Trapped	< 0	< 0
Marginally trapped	0	< 0
Outer trapped	< 0	anything
Marginally outer trapped	0	anything
Weakly trapped	≤ 0	≤ 0

Table 3.1: Definition of different types of trapped surfaces in terms of the null expansions.

a positive factor σ so that $\vec{k}_+ \to \sigma\vec{k}_+$, $\vec{k}_- \to \vec{k}_-/\sigma$, without changing the normalization. However, this will not affect the *signs* of the null expansions. This is a good thing, since it is the signs of the null expansions that determine if the surface is trapped or not; we are not really interested in their exact values.

Besides the purely trapped surfaces there are relatives in the form of marginally trapped, outer trapped, and marginally outer trapped surfaces. In general, they are all *weakly trapped*. The terminology is made clear in Table 3.1 in terms of the null expansions. For a more extensive classification of surfaces, see [26].

3.2 Horizons

Now that we have defined what trapped surfaces are, let us come back to the question of what makes them interesting. Trapped surfaces lay the ground for a number of singularity theorems; in particular, see the theorems by Penrose [23], and Hawking and Penrose [27]. These theorems show that certain physically reasonable assumptions lead to geodesic incompleteness. Thus, the presence of singularities is believed to be a generic feature in the context of gravitational collapse as well as in cosmology. A singularity is predicted in the future of a trapped surface. The cosmic censorship hypothesis then suggests that there is an event horizon. Thus, the presence of a trapped surface indicates that a black hole has been formed, even though the exact evolution of spacetime is unknown. Moreover, the location of a trapped surface is related to that of the event horizon. Assuming that cosmic censorship holds, trapped surfaces can only exist inside an event horizon [28]. Thus, if a trapped surface were to be observed, it would be so inside a black hole.[1] This fact has given hope to the possibility of a new definition of black holes, and definitions of various kinds of horizons have come about [29].

In Hawking's definition of an *apparent horizon* spacetimes foliated by

[1]However, there are no general theorems stating that trapped surfaces must form in a gravitational collapse to a black hole.

asymptotically flat, spacelike hypersurfaces Σ_t are considered [28]. The *trapped region* on such a hypersurface is defined as the set of all points such that an outer trapped surface in Σ_t passes through it. The apparent horizon is then defined as the boundary of the trapped region. It could thus be regarded as the instantaneous boundary of a black hole.

In numerical relativistic simulations, spacetimes are constructed through evolutions of initial data hypersurfaces. In such simulations the infinite future—and thus the location, if any, of an event horizon—is unknown. In this context the term *apparent horizon* has a slightly different meaning [30]. On a given spatial hypersurface, all (marginally) outer trapped surfaces can be found. Here, the outermost marginally outer trapped surface on the spatial slice is called the apparent horizon. In the practice of numerical relativity, the apparent horizon serves as the definition of the boundary of a black hole. The importance of trapped surfaces in numerical relativity thus constitutes a strong motivation for the study of these.

Both of the above definitions of an apparent horizon are highly dependent on the given spatial slicing of the spacetime. There may exist trapped surfaces—lying not in one of the given spatial slices—that extend beyond the apparent horizon. For instance, there are slicings of the Schwarzschild spacetime, reaching the singularity, which fail to include a trapped surface in any spatial slice [31], even though the whole interior of the Schwarzschild black hole is filled with trapped surfaces.

Many important horizons are built from marginally (outer) trapped surfaces. A hypersurface foliated by marginally (outer) trapped surfaces is referred to as a *marginally (outer) trapped tube*.

An *isolated horizon* [32] is a null hypersurface foliated by marginally outer trapped surfaces, with extra conditions imposed. It is "isolated" in the sense that it does not interact with its surroundings. In a dynamical situation the area of a black hole is expected to grow. Thus, the notion of an isolated horizon may be complemented by that of a *dynamical horizon* [32], which is intended to model an evolving black hole. A dynamical horizon is a *spacelike* marginally trapped tube. A first step to provide an analytically exact model of such an evolution of a marginally trapped tube is given in Paper I. Here, we see that the isolated horizon makes a sudden jump outwards in a spacelike direction as matter is falling into the black hole. However, this marginally trapped tube is discontinuous, and does not contain a spacelike portion. But possibly, a dynamical horizon could be provided by a refinement of the model.

The event horizons of the stationary Schwarzschild and Reissner-Nordström solutions are isolated horizons. In fact, every Killing horizon with the required topology is an isolated horizon. A Killing horizon is not necessarily a black hole horizon, and neither is an isolated horizon. The concept of isolated horizons thus applies to a wider class of horizons, not only event horizons.

A *trapping horizon* [33] is a marginally trapped tube with an extra requirement making sure that there are trapped surfaces in its vicinity. It is either spacelike or null. A trapping horizon may be *future* trapped or *past* trapped, depending on if it is foliated by future or past marginally trapped surfaces. If the congruence of light rays having zero expansion on the horizon diverges just outside the horizon and converges just inside, the trapping horizon is said to be *outer*, and vice versa for an *inner* trapping horizon. Applying these concepts to the Reissner-Nordström solution, we find that the event horizon is a *future outer* trapping horizon, the inner horizon is a future *inner* trapping horizon, while the white hole horizons are *past* outer/inner trapping horizons. The existence of a black hole could very well be defined by the presence of a future outer trapping horizon.

3.3 A boundary

One possible drawback of all the horizons described in the previous section is that they are not in any way uniquely defined [34]. Instead one could define a *trapping boundary* [33] as the boundary of the region containing trapped surfaces in the *full* spacetime. But it has proven to be a quite difficult task to find this boundary, even in simple spacetime models.

In spherically symmetric spacetimes, it is possible to at least define a *past barrier*: a spacelike hypersurface to the past of which no future trapped surface can lie. In such a spacetime, there are preferred round spheres with area radius r. Provided that r is not everywhere constant, r can be used as a coordinate. The metric then takes the general form

$$ds^2 = -e^{2\beta}\left(1 - \frac{2m}{r}\right)dt^2 + \left(1 - \frac{2m}{r}\right)^{-1} dr^2 + r^2 d\Omega^2. \tag{3.8}$$

The function $\beta(t, r)$ has no physical meaning. The *Misner-Sharp mass* $m(t, r)$, on the other hand, does. It is defined as

$$1 - \frac{2m(t, r)}{r} = g^{ab}\nabla_a r \nabla_b r. \tag{3.9}$$

In a static spacetime m and β are functions of r only. For example, the Schwarzschild and Reissner-Nordström metrics (2.1) are given with $\beta = 0$, and $m = M$ (constant) in the Schwarzschild case, and $m = m(r)$ in the Reissner-Nordström case. The round spheres of constant t and r are trapped if $r < 2m$ and marginally trapped if $r = 2m$.

A *Kodama vector field* $\vec{\xi}$ can be defined as follows:

- $\vec{\xi}$ is orthogonal to the round spheres,
- $\xi^a \nabla_a r = 0$, that is, the area of the round spheres is constant in the direction of $\vec{\xi}$,

- $||\vec{\xi}||^2 = -g^{ab}\nabla_a r \nabla_b r$.

The Kodama vector field is necessarily hypersurface orthogonal, so that there is some function τ which is constant on hypersurfaces orthogonal to $\vec{\xi}$. Note that, from the normalization of $\vec{\xi}$, it follows that $\vec{\xi}$ is timelike where $r > 2m$, null where $r = 2m$, and spacelike where $r < 2m$. Whenever $\vec{\xi}$ is timelike, hypersurfaces of constant τ are spacelike, and τ is referred to as *Kodama time*, giving a natural notion of time. We set it up so that $\vec{\xi}$ is future directed whenever it is timelike, and so that τ increases in the direction of $\vec{\xi}$.

Now, under certain reasonable restrictions on the mass function m, a trapped surface can not have a minimum in Kodama time, nor can any open portion of it lie in a hypersurface of constant τ. Thus a past barrier can be defined as the last hypersurface of constant τ which is nowhere timelike [35]. The value of τ on the past barrier is the maximum value that the Kodama time takes on the event horizon. No trapped surface can extend to the past of this barrier, or even touch it.

In Paper II weakly trapped surfaces are explicitly constructed in the Oppenheimer-Snyder model. They are designed so as to pass through the centre of the dust cloud at earliest possible time. Even though we have no proof that the surfaces we found are optimal—although we believe that they are close to the trapping boundary—at least, they set a temporal upper bound for the location of the trapping boundary. Together with the identification of the past barrier, the region where the trapping boundary of this model can possibly be located has been narrowed down.

3.4 Can a trapped surface be seen?

We end this thesis with an interesting question. Suppose that an observer is falling into a black hole, while light is emitted from a trapped surface inside the black hole. Will the observer be able to detect the light signals, finding out that the surface is trapped—and thus knowing that s/he is inside a black hole—before crashing into the singularity?

In a Schwarzschild black hole, the answer is given by Wald and Iyer [31]. Every sphere of constant t and r inside a Schwarzschild black hole is trapped. Imagine observers spread out over such a sphere; in particular one observer sitting at the north pole, and one observer sitting at the south pole, measuring the expansion of light from where they are sitting. In order for the observers to tell if the sphere is trapped, they must be able to tell each other of their findings. That is, the observers at the south and north poles must be in causal contact. However, it turns out that they are not. The observer at the north pole will hit the singularity before s/he is reached by a light signal from the south pole. Thus, in this case, the answer to the question proposed in the title of this section is no.

In fact, the proof of Wald and Iyer is more general than the above example. Consider a timelike curve γ in the Schwarzschild spacetime, intersecting round spheres of the spacetime at the north pole, and terminating at the singularity. The chronological past $I^-(\gamma)$ of γ is defined as the set of all points from which a timelike curve can reach γ. In this case, with γ ending at the singularity, $I^-(\gamma)$ is called a *terminal indecomposable past set* (TIP). It can be proven that no trapped surface—any trapped surface, not only a round sphere—lies in the chronological past of γ. This fact can be used to define a spatial slicing of the Schwarzschild spacetime with no apparent horizon. Further, it is argued that no trapped surface can lie even in the *causal past* of γ, consisting of the set of points from which a *lightlike* curve can reach γ. Thus no trapped surface can be seen by an observer sitting at the north pole (or any other point of the sphere).

A similar calculation can be carried out in the charged Reissner-Nordström black hole. There, the answer will be that no trapped sphere can be seen by an observer before the inner horizon is reached. If the instability of the inner horison would give rise to a singularity there, then no round trapped sphere could be seen in the Reissner-Nordström black hole either.

In general, however, it is not true that a trapped surface can never be seen by an observer. In the more physical Oppenheimer-Snyder model, for example, trapped spheres may be seen by an observer sitting at the centre of the dust cloud. This may perhaps become more apparent to the reader turning to the accompanying papers.

Bibliography

[1] T. W. Baumgarte and S. L. Shapiro *Numerical Relativity: Solving Einstein's Equations on the Computer* (Cambridge University Press, Cambridge, 2010)

[2] R. Penrose in *Battelle Rencontres: 1967 lectures in mathematics and physics*, ed. C M DeWitt and J A Wheeler (W. A. Benjamin, New York, 1968)

[3] E. Jakobsson *Trapped Surfaces in 2+1 dimensions*, Master's Thesis, Stockholm University, 2011

[4] K. Schwarzschild *Sitzber. Deut. Akad. Wiss. Berlin*, Kl. Math.-Phys. Tech. 189 (1916)

[5] A. Einstein *Preuss. Akad. Wiss. Berlin, Sitzber.* 844 (1915)

[6] D. Finkelstein *Phys. Rev.* **110** (1958) 965

[7] M. D. Kruskal *Phys. Rev.* **119** (1960) 1743

[8] M. Walker *J. Math. Phys.* **11** (1970) 2280

[9] H. Reissner *Ann. Physik* **50** (1916) 106

[10] G. Nordström *Proc. Kon. Ned. Akad. Wet.* **20** (1918) 1238

[11] J. C. Graves and D. R. Brill *Phys. Rev.* **120** (1960) 1507

[12] E. Poisson and W. Israel *Phys. Rev.* **D41** (1990) 1796

[13] M. Dafermos *Commun. Pure Appl. Math.* **58** (2005) 445

[14] I. Bengtsson, S. Holst, and E. Jakobsson. Work in progress.

[15] R. P. Kerr *Phys. Rev. Lett.* **11** (1963) 237

[16] E. T. Newman, E. Couch, K. Chinnapared, A. Exton, A. Prakash and R. Torrence *J. Math. Phys.* **6** (1965) 918

[17] B. O'Neill *The Geometry of Kerr Black Holes* (A K Peters, Wellesley, Massachusetts, 1995)

[18] J. R. Oppenheimer and H. Snyder *Phys. Rev.* **56** (1939) 455

[19] A. Friedmann *Z. Phys.* **10** (1922) 377

[20] E. Poisson *A Relativist's Toolkit: The Mathematics of Black-Hole Mechanics* (Cambridge University Press, Cambridge, 2004)

[21] D. Christodoulou *Commun. Math. Phys.* **93** (1984) 171

[22] S. A. Hayward in *Proceedings of the Ninth Marcel Grossmann Meeting*, ed. V. G. Gurzadyan *et al.* (World Scientific, Singapore, 2002)

[23] R. Penrose *Phys. Rev. Lett.* **14** (1965) 57

[24] C. W. Misner in *Relativity Theory and Astrophysics I: Relativity and Cosmology*, ed. J. Ehlers, Lectures in Applied Mathematics, Vol. **8** (American Mathematical Society, Providence, 1967)

[25] M. Bañados, M. Henneaux, C. Teitelboim and J. Zanelli *Phys. Rev.* **D48** (1993) 1506

[26] J. M. M. Senovilla *Class. Quant. Grav.* **24** (2007) 3091

[27] S. W. Hawking and R. Penrose *Proc. Roy. Soc* **A314** (1970) 529

[28] S. W. Hawking and G. F. R. Ellis *The Large Scale Structure of Space-Time* (Cambridge University Press, Cambridge, 1973)

[29] I. Booth *Can. J. Phys.* **83** (2005) 1073

[30] T. W. Baumgarte and S. L. Shapiro *Physics Reports* **376** (2003) 41

[31] R. M. Wald and V. Iyer *Phys. Rev.* **D44** (1991) R3719

[32] A. Ashtekar and B. Krishnan *Living Rev. Rel.* **7** (2004) 10 (www.livingreviews.org/lrr-2004-10)

[33] S. A. Hayward *Phys. Rev.* **D49** (1994) 6467

[34] A. Ashtekar and G. J. Galloway *Adv. Theor. Math. Phys.* **9** (2005) 1

[35] I. Bengtsson and J.M.M. Senovilla *Phys. Rev.* **D83** (2011) 044012

Paper I

IOP PUBLISHING CLASSICAL AND QUANTUM GRAVITY

Class. Quantum Grav. **30** (2013) 065022 (7pp) doi:10.1088/0264-9381/30/6/065022

How trapped surfaces jump in 2 + 1 dimensions

Emma Jakobsson

Fysikum, Stockholms Universitet, SE-106 91, Stockholm, Sweden

E-mail: emma.jakobsson@fysik.su.se

Received 10 September 2012, in final form 6 February 2013
Published 1 March 2013
Online at stacks.iop.org/CQG/30/065022

Abstract
When a lump of matter falls into a black hole it is expected that a marginally trapped tube when hit moves outwards everywhere, even in regions not yet in causal contact with the infalling matter. But to describe this phenomenon analytically in 3 + 1 dimensions is difficult since gravitational radiation is emitted. By considering a particle falling into a toy model of a black hole in 2 + 1 dimensions an exact description of this non-local behaviour of a marginally trapped tube is found.

PACS number: 04.20.−q

1. Introduction

A black hole is defined by its event horizon; a boundary in spacetime, such that no event inside it can ever be seen from the outside. With this definition it is impossible to locate the event horizon without knowledge about the infinite future. Attempts to make alternative definitions of a black hole involve trapped surfaces that occur in the interior [1–3]. A trapped surface is a closed, spacelike surface such that both families of light rays orthogonal to it converge. The terminology of concepts closely related to these trapped surfaces might need to be made clear: A closed spacelike surface such that only one of the orthogonal families of light rays converges while the other has zero convergence, is referred to as a *marginally* trapped surface. If the surface is embedded in a hypersurface on which an outer direction is defined in a manner that would be intuitive in an asymptotically simple spacetime, and this surface is such that the outgoing family of light rays orthogonal to it converges, it is called *outer* trapped, regardless of the behaviour of the ingoing family of light rays. *Marginally outer* trapped surfaces are defined in a similar manner. While the event horizon is a globally defined property of spacetime—and therefore, as we will see, teleological in its nature—trapped surfaces are quasilocal, since their definition only involves the surfaces themselves and their infinitesimal surroundings. For this reason trapped surfaces are of importance to numerical relativists, since the occurrence of such is the only practical way to identify a black hole in a simulated evolution of spacelike hypersurfaces. In such simulations the trapped surfaces

0264-9381/13/065022+07$33.00

sometimes make discontinuous 'jumps' outwards [4, 5]. This phenomenon is expected when matter is falling into the black hole [6].

A *marginally trapped tube* is a hypersurface foliated by marginally trapped surfaces. The marginally trapped tubes we will come across will be null and satisfy some other constraints that qualify them as isolated horizons [7]. It is desirable to find an exact description of how a marginally trapped tube is affected when hit by matter. This problem has also been studied in spherically symmetric cases [8, 9]. However, if a localized 'lump' of matter is falling into a black hole, it is much more difficult to find an analytical description since gravitational radiation is emitted. But it is expected that the jump in this case will be in some sense non-local; that the jump will take place also in regions not yet in causal contact with the infalling matter. There is no need to worry about causality violation; this effect is just a consequence of the quasilocal definition of a trapped surface. Light rays emitted from a region on a spacelike surface may converge, but whether the whole surface is closed—and thus trapped—or not depends on circumstances elsewhere.

Because of the difficulties in 3+1 dimensions we instead tackle the problem in 2+1 dimensions where there is no gravitational radiation. We consider a toy model of a black hole and let a point particle fall into it in order to find an exact description of how the marginally trapped tube jumps outwards in this non-local way.

2. The black hole and trapped surfaces

The existence of a black hole in a 2+1-dimensional spacetime with constant negative curvature was first discovered by Bañados *et al* [10]. This is called a BTZ black hole. It is obtained by identifying points in anti-de Sitter space using an isometry [11].

2+1-dimensional anti-de Sitter space can be defined as the hypersurface

$$X^2 + Y^2 - U^2 - V^2 = -1, \tag{1}$$

embedded in a four dimensional spacetime with metric

$$\mathrm{d}s^2 = \mathrm{d}X^2 + \mathrm{d}Y^2 - \mathrm{d}U^2 - \mathrm{d}V^2. \tag{2}$$

It has constant curvature which is negative. Each point can be represented by a matrix

$$\boldsymbol{g} = \begin{pmatrix} U+Y & X+V \\ X-V & U-Y \end{pmatrix}, \tag{3}$$

so that

$$\det \boldsymbol{g} = -X^2 - Y^2 + U^2 + V^2 = 1. \tag{4}$$

But this is a group element of $SL(2,\mathbb{R})$, consisting of all two by two matrices with real matrix elements and determinant one. Furthermore, any isometry can be described by letting the group act on itself. Isometries leaving the unit element fixed can be written

$$\boldsymbol{g} \to \boldsymbol{g}' = \boldsymbol{g}_1 \boldsymbol{g} \boldsymbol{g}_1^{-1}, \tag{5}$$

where $\boldsymbol{g}_1 \in SL(2,\mathbb{R})$. Transformations of the type (5) will have a line of fixed points and the nature of this line is determined by the trace of $\boldsymbol{g}_1$. If $\mathrm{Tr}\,\boldsymbol{g}_1 < 2$ it will be timelike, if $\mathrm{Tr}\,\boldsymbol{g}_1 = 2$ it will be lightlike and if $\mathrm{Tr}\,\boldsymbol{g}_1 > 2$ it will be spacelike.

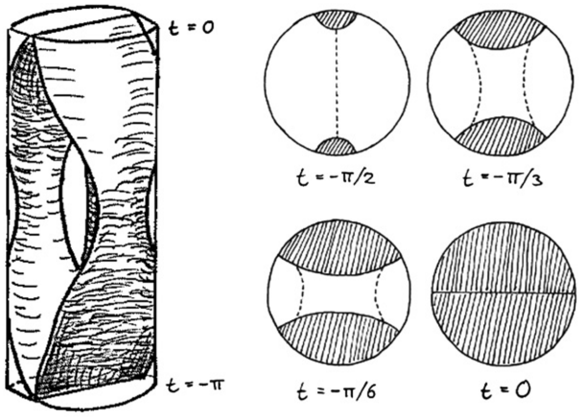

Figure 1. The BTZ black hole. The cylinder is depicting 2+1-dimensional anti-de Sitter space in which the identification surfaces are drawn. To the right are spatial slices with different values of constant t. As the identification is performed the shaded regions are cut away, and each slice, except $t = 0$, turns into a cylinder with two asymptotic regions. In this figure, only the top left disk where $t = -\pi/2$ will turn into a smooth surface by the identification, since the flow lines of the identification in general do not lie on a disk of constant t. But the full spacetime is smooth everywhere except at the singularity, drawn on the bottom right disk where $t = 0$. The dashed curves on the disks are the event horizons—one for each asymptotic region. (This figure is a paraphrase on a figure originally drawn by Holst [13].)

The embedding coordinates are convenient to use in calculations, but for visualization the intrinsic coordinates (t, ρ, ϕ) [12] are a better choice. They are given by

$$\begin{aligned} X &= \frac{2\rho}{1-\rho^2}\cos\phi \\ Y &= \frac{2\rho}{1-\rho^2}\sin\phi \qquad \begin{array}{l} 0 \leqslant \rho < 1 \\ 0 \leqslant \phi < 2\pi \end{array} \\ U &= \frac{1+\rho^2}{1-\rho^2}\cos t \qquad -\pi \leqslant t < \pi . \\ V &= \frac{1+\rho^2}{1-\rho^2}\sin t \end{aligned} \tag{6}$$

The metric in these coordinates is

$$\mathrm{d}s^2 = -\left(\frac{1+\rho^2}{1-\rho^2}\right)^2 \mathrm{d}t^2 + \frac{4}{(1-\rho^2)^2}(\mathrm{d}\rho^2 + \rho^2 \mathrm{d}\phi^2). \tag{7}$$

With this choice of coordinates anti-de Sitter space is depicted as a cylinder. The timelike coordinate t runs along the cylinder, and the spatial slices of constant t are Poincaré disks. On the disk, ρ and ϕ are the radial and angular coordinates respectively and $\mathcal{J}$ is situated at the boundary $\rho = 1$.

To create a black hole we choose a group element

$$\boldsymbol{g}_{\mathrm{BH}} = \begin{pmatrix} \cosh\mu & \sinh\mu \\ \sinh\mu & \cosh\mu \end{pmatrix}. \tag{8}$$

The real constant μ will determine the mass of the black hole. Then we act with $\boldsymbol{g}_{\mathrm{BH}}$ on anti-de Sitter space through conjugation as in equation (5), and identify points that are transformed into each other. The region between the two surfaces $Y = V \tanh\mu$ and $Y = -V \tanh\mu$ can be taken to represent the resulting quotient space, as in figure 1. Due to the identification a spacelike slice now has the geometry of a cylinder, but space is still locally anti-de Sitter everywhere. Note that there are two asymptotic regions, as in the Schwarzschild solution in which one of the regions is considered unphysical. The fixed points of the transformation yielding the identification are located at the spacelike line $Y = V = 0$. Starting from the slice $t = -\pi/2$ it is seen that the cylinders shrink in the periodical direction as t increases, until one dimension suddenly disappears at $t = 0$, and all that is left is the line of fixed points. A geodesic ending at this singular line ends after only a finite parameter time, meaning that this spacetime is geodesically incomplete. The event horizon is the backward light cone of the last point on $\mathcal{J}$, i.e. the point where the singular line meets $\mathcal{J}$. There is one event horizon for each asymptotic region. In the embedding coordinates the event horizons are given as the quotient of each of the two surfaces $X = \pm U$.

The black hole spacetime is locally anti-de Sitter everywhere except at the singular line. On a spacelike surface, the only way to distinguish it from anti-de Sitter space is through the holonomy of the black hole: If a vector is parallel transported along a curve closed by the identification it will also be transformed by the group element effecting the identification.

Finding trapped surfaces—or rather trapped curves, since we are in 2+1 dimensions—is easy. Consider the intersection of two light cones with vertices at the singularity. Light rays emanating orthogonally from such curves obviously converge. Moreover they coincide with flow lines of the identifying isometry and are therefore closed to smooth curves by the identification. Hence they are trapped. By letting one of the two vertices be on $\mathcal{J}$, and varying the other, it is easily seen that the event horizon is a marginally trapped tube, that is a surface foliated by marginally trapped curves. Since trapped surfaces can not exist outside the event horizon according to the cosmic censorship hypothesis, the marginally trapped tube—that is the event horizon in this model—is also the boundary of the region containing trapped curves.

In fact this is the complete picture: all marginally trapped curves lie on the event horizon. To see this, consider Raychaudhuri's equation [14] for the expansion θ of a congruence of lightlike geodesics in 2+1 dimensions. With k^a being the tangent vector of a given geodesic we have

$$\dot{\theta} = -\theta^2 - R_{ab}k^a k^b. \tag{9}$$

If we impose Einstein's vacuum equation $R_{ab} = \lambda g_{ab}$ the second term vanishes since $k^2 = 0$ for a lightlike geodesic. We are left with

$$\dot{\theta} = -\theta^2, \tag{10}$$

which shows that a congruence of lightlike geodesics that have zero convergence at some point, must continue to have zero convergence. The conclusion is that a marginally trapped curve must lie on a null plane[1], where a null plane is defined as a light cone with its vertex on $\mathcal{J}$. It is not difficult to show that only the null plane containing a fixed point on $\mathcal{J}$ contains smooth and spacelike closed curves.

As a side note, there is a theorem that says that a region of a spacelike hypersurface bounded by an outer trapped surface in one direction and by an outer untrapped surface in the other must contain a marginally outer trapped surface [15]. In this model the statement is almost obvious. Any smooth spacelike surface passing through the interior of the black hole will contain a smooth closed curve lying on the event horizon and thus being a marginally outer trapped curve. Since it lies on the event horizon it also separates the region containing trapped curves from the region not containing trapped curves on the surface.

[1] This does not hold in 3+1 dimensions, since Raychaudhuri's equation will then contain extra terms.

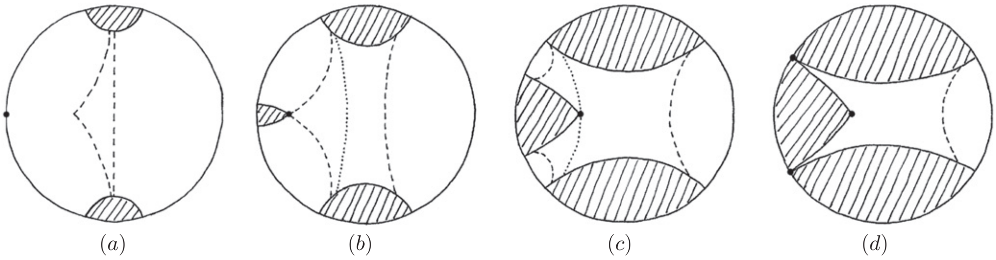

Figure 2. A sequence of Poincaré disks shows what happens when the particle falls into the black hole (compare with figure 3). (*a*) The particle comes in from infinity. The event horizon has a kink and does not contain any marginally trapped curves. (*b*) The particle meets the event horizon which from here on is a smooth marginally trapped tube. The dotted curve is the isolated horizon that would have been the event horizon had the particle not been there. (*c*) The isolated horizon in the inner region is hit by the particle. From this point on it ceases to be a smooth marginally trapped tube. (*d*) A fixed point appears on $\mathcal{J}$ as the identification surfaces of the particle and the black hole begin to intersect. The dashed curve to the right is not relevant in these figures; it is just an artefact of the other asymptotic region.

3. The infalling particle

Just like a black hole was obtained by identifying points, a point particle can be modelled using the same trick. Note that the matrix of equation (8) has a trace larger than two, and therefore has a spacelike line of fixed points. If we instead choose the group element

$$\boldsymbol{g}_P = \begin{pmatrix} 1 & 2a \\ 0 & 1 \end{pmatrix}, \tag{11}$$

with a being an arbitrary real constant, and identify points in anti-de Sitter space through conjugation, the line of fixed points will be lightlike since $\mathrm{Tr}\,\boldsymbol{g}_P = 2$. A fundamental region containing one representative of every point in the quotient space can be chosen by cutting away the wedge between the two identified surfaces $Y = \pm a(X - V)$. The effect is that a surface of constant t now has the geometry of a cone, with the tip of the cone being a fixed point of the identification. This setup perfectly well describes a point particle [16, 17]. The particle is situated at the conical singularity, and it is a lightlike particle since its world line is lightlike. Let us consider a sequence of Poincaré disks. Before the time $t = -\pi/2$ there is no particle, just empty anti-de Sitter space. At $t = -\pi/2$ the particle comes in from infinity. Then it traverses the disk as t increases until it finally leaves at $t = \pi/2$ and we again are left with empty anti-de Sitter space. On the disk, space is locally anti-de Sitter everywhere except at the singularity, and the only way to notice the presence of the particle is to travel around it and reveal its holonomy. That the particle enters empty anti-de Sitter space from infinity is a property unique for lightlike particles in this construction. It is not crucial that the particle we use is lightlike, we might just as well consider a timelike particle. But the advantage of using a lightlike particle is that the starting point will be an undisturbed BTZ spacetime, instead of a white hole emitting massive particles.

We are now ready to set up a model in which we let the particle fall into the black hole. The result is illustrated in figure 2. As the lightlike particle approaches the centre of the disk it is seen how the identification surfaces of the particle eventually begin to intersect the identification surfaces of the black hole. These points of intersection are fixed points under the action of the combined holonomy $\boldsymbol{g}_{\mathrm{tot}} = \boldsymbol{g}_P\boldsymbol{g}_{\mathrm{BH}}$. Here the constants a and μ are chosen so that $|\mathrm{Tr}\,\boldsymbol{g}_{\mathrm{tot}}| > 2$ and consequently the transformation $\boldsymbol{g} \to \boldsymbol{g}_{\mathrm{tot}}\boldsymbol{g}\boldsymbol{g}_{\mathrm{tot}}^{-1}$ has a spacelike line of fixed points. This spacelike line is singular and appears at smaller t than the singularity of the

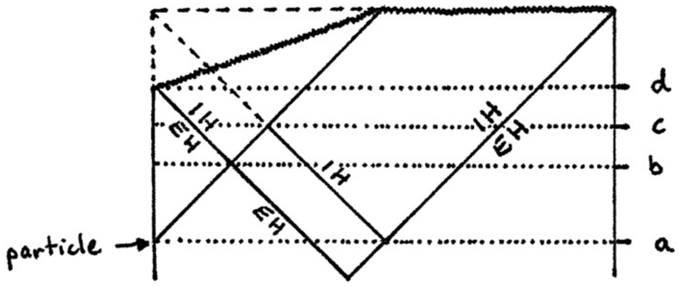

Figure 3. A conformal diagram of our model clearly illustrates how the isolated horizon 'jumps' outwards when it is hit by the particle. The dashed lines show the location of the singularity and the event horizon had the particle not been there. The light cone on which the path of the particle lies splits the spacetime into two different regions. In the outer region the isolated horizon foliated by marginally trapped curves coincides with the event horizon, and in the inner region it does not.

original black hole. This means that the role of the original singularity is taken over by this new singular line. In turn this affects the location of the event horizon, shown as the dashed curves in figure 2. Also the mass of the black hole has been affected by the infalling particle. The change in mass is determined by the constant a.

It turns out that the event horizon in this model has a kink before the particle crosses it. This kink nicely illustrates the teleological nature of the event horizon since it has acquired a kink not because of something that has happened to it in the past, but because of something that will happen to it in the future.

Due to the kink the event horizon is not everywhere smooth, with the consequence that it is not completely foliated by marginally trapped curves. The question now is where the marginally trapped curves are in this model. We know that they are found on null planes and that a null plane is smooth only if it contains a fixed point on $\mathcal{J}$. It is a crucial fact that the light cone on which the path of the particle lies splits the spacetime into two qualitatively different parts.

In the outer region the holonomy is $\boldsymbol{g}_{\mathrm{tot}}$. The event horizon is smooth and it contains the point on $\mathcal{J}$ that is a fixed point under the action of this holonomy. Therefore it is also foliated by marginally trapped curves. Moreover, the event horizon is the boundary of the region containing trapped curves since these can only appear in the interior of the black hole.

In the inner region, on the other hand, the holonomy is $\boldsymbol{g}_{\mathrm{BH}}$, and it is therefore isometric to a region of the BTZ spacetime. Restricted to this region, the situation is thus identical to that of a black hole with no infalling particle. All marginally trapped curves lie on the null plane that would have been the event horizon had the particle not been there. And, as we saw, this null plane is also the boundary of the region containing trapped curves. It is an isolated horizon in the terminology of [7], as well as the event horizon in the outer region. But after it has been hit by the particle—in the outer region—it is no longer smooth.

The marginally trapped tube thus consists of two parts: the two isolated horizons in the inner and the outer region respectively. All marginally trapped curves lie on the marginally trapped tube, and thus we have a complete knowledge of their whereabouts, independent of a given foliation of spacetime. When the particle hits the isolated horizon in the interior of the black hole, it is seemingly destroyed but then reappears on the event horizon in the outer region, it 'jumps'. This is clearly illustrated in the conformal diagram of figure 3. With this model in which the marginally trapped tube is discontinuous we have thus found a reasonable and exact illustration of how marginally trapped curves jump when hit by matter.

4. Conclusions

By considering a toy model of a black hole in 2+1 dimensions and letting a point particle fall into the black hole, we have seen how the marginally trapped tube splits into two parts. This exact description of the splitting illustrates the non-local jump described in the introduction. Similarly non-local jumps are expected in 3+1 dimensions, but most likely that case must be attacked numerically.

As a concluding remark it is worth noting that since the world line of the particle is singular, the two parts of the marginally trapped tube can not be connected. To get around this problem one could consider a small tube of null dust instead of a point particle. It might be interesting to see what the marginally trapped tube would look like in this more complicated model; in particular if it would be smooth, and if so, if the smooth part joining the two isolated horizons would be timelike or spacelike.

Acknowledgments

I would like to thank Ingemar Bengtsson for bringing my attention to the problem and for his significant support, and two anonymous referees for helpful comments. I would also like to thank Sören Holst for accepting the similarities between figure 1 and his original.

References

[1] Hayward S A 2002 *Proc. 9th Marcel Grossmann Meeting* ed V G Gurzadyan *et al* (Singapore: World Scientific) p 568
[2] Ashtekar A and Krishnan B 2004 *Living Rev. Rel.* **7** 10 (available at www.livingreviews.org/lrr-2004-10)
[3] Booth I 2005 *Can. J. Phys.* **83** 1073
[4] Andersson L, Mars M and Simon W 2005 *Phys. Rev. Lett.* **95** 111102
[5] Jaramillo J L, Ansorg M and Vasset N 2009 *AIP Conf. Proc.* **1122** 308
[6] Hawking S W and Ellis G F R 1973 *The Large Scale Structure of Space-Time* (Cambridge: Cambridge University Press)
[7] Ashtekar A, Dreyer O and Wisniewski J 2002 *Adv. Theor. Math. Phys.* **6** 507 (arXiv:gr-qc/0206024)
[8] Ben-Dov I 2004 *Phys. Rev.* D **70** 124031
[9] Booth I, Brits L, Gonzalez J A and Van Den Broeck C 2006 *Class. Quantum Grav.* **23** 413
[10] Bañados M, Teitelboim C and Zanelli J 1992 *Phys. Rev. Lett.* **69** 1849
[11] Bañados M, Henneaux M, Teitelboim C and Zanelli J 1993 *Phys. Rev.* D **48** 1506
[12] Holst S 2000 Horizons and time machines *PhD Thesis* Stockholm University
[13] Åminneborg S, Bengtsson I, Holst S and Peldán P 1996 *Class. Quantum Grav.* **13** 2707
[14] Wald R M 1984 *General Relativity* (Chicago, IL: University of Chicago Press)
[15] Andersson L and Metzger J 2009 *Commun. Math. Phys.* **290** 941
[16] Deser S, Jackiw R and 't Hooft G 1984 *Ann. Phys.* **152** 220
[17] Deser S and Steif A 1992 *Class. Quantum Grav.* **9** L153

Paper II

PHYSICAL REVIEW D **88,** 064012 (2013)

Trapped surfaces in Oppenheimer-Snyder black holes

Ingemar Bengtsson,[1,*] Emma Jakobsson,[1,†] and José M. M. Senovilla[2,‡]

[1]*Stockholms Universitet, Fysikum, AlbaNova, S-106 91 Stockholm, Sweden*

[2]*Física Teórica, Universidad del País Vasco, Apartado 644, 48080 Bilbao, Spain*

(Received 16 July 2013; published 5 September 2013)

The Oppenheimer-Snyder solution models a homogeneous round dust cloud collapsing to a black hole. Inside its event horizon there is a region through which trapped surfaces pass. We try to determine exactly where the boundary of this region meets the center of the cloud. We present explicit examples of the relevant trapped (topological) spheres; they extend into the exterior vacuum region, and are carefully matched at the junction between the cloud and the vacuum.

DOI: 10.1103/PhysRevD.88.064012 PACS numbers: 04.70.Bw

I. INTRODUCTION

In spacetime terms the boundary of a black hole is—according to a definition which may need refinement [1–3]—its event horizon. According to Penrose's singularity theorem [4] it is the appearance of trapped surfaces that really spells the doom of the collapsing matter. The event horizon is added as an afterthought by a cosmic censor. Indeed, in numerical relativity, the signal for a black hole is the presence of outer trapped surfaces on a given spatial slice [5]. In a dynamical situation these typically lie well inside the event horizon, but by considering all possible slicings outer trapped surfaces can probably be found passing through every point inside the event horizon [6], while trapped surfaces cannot [7]. The distinction between trapped and outer trapped surfaces comes about because the latter are required to be (weakly) trapped, that is, to have (nonpositive) negative future null expansions both outwards and inwards, thus obviating the need for using a spatial hypersurface to provide the meaning of "outer." In this paper we are concerned with (weakly) trapped surfaces only.

The boundary of the region where trapped surfaces occur [8] is remarkably difficult to determine [9]. This is true also for the simplest possible models of matter collapsing to form black holes: the Oppenheimer-Snyder (OS) and Vaidya solutions. Both of them are spherically symmetric, and are constructed by matching regions with collapsing matter to vacuum regions. They both have a central world line surrounded by a tube of round marginally trapped surfaces (MTSs). In the Vaidya model this tube is spacelike, is composed of outermost stable MTSs (in a technical sense [10]), and lies outside the causal past of the central world line. In the OS model the tube is timelike, is composed of unstable MTSs, and is visible in its entirety from the central world line. In some ways therefore the two models behave very differently. In the inhomogeneous Lemaître-Tolman-Bondi models [11] both kinds of behavior are observed [12]. An achronal spherically symmetric tube of MTSs asymptotic to the event horizon will exist provided certain conditions on the stress-energy tensor are met [13].

Trapped surfaces are compact without boundary; in particular, we will consider topological spheres, but they do not have to be round, so we can still ask whether there are trapped surfaces intersected by the central world line. For the Vaidya model, with some conditions on the rate of infall of matter, the answer is yes [14], even though in this case the central world line never encounters nonzero spacetime curvature. Here we address the same question for the OS model. Since the answer to the first question is again yes, we go on to ask at what value of proper time along the central world line are trapped surfaces first encountered. We believe that we know the answer to this question too, but will not be able to offer a conclusive proof. At least, we have taken a step towards determining the location of the boundary of the trapped region in this model.

In the construction of the models the matching of the matter-filled regions to the vacuum regions is done in such a way that the spacetime metric is C^1, but this is not manifest in the coordinate descriptions used. We will insist that the trapped surfaces we consider have the same degree of differentiability. In the earlier paper on the Vaidya model [14] this issue was not properly addressed, but then the question was not very critical either because no attempt to optimize the construction was made there. For our purposes here it is crucial to handle this issue with care, and we explain the rules in a separate Appendix.

We begin the story in Sec. II by describing the Oppenheimer-Snyder solution in some detail, and comparing it to the Vaidya solution. Section III contains some preliminary discussion of trapped surfaces confined within the dust cloud. In Sec. IV we introduce the class of trapped surfaces that we believe are the best if one wants them to reach the center of the cloud at the earliest possible times. We also calculate what we believe to be the earliest possible time. This is a main result of our paper. Some of the trapped surfaces are built explicitly and we want to remark

*ibeng@fysik.su.se
†emma.jakobsson@fysik.su.se
‡josemm.senovilla@ehu.es

that they are probably difficult to be found in numerical approaches. In Sec. V we present partial proofs that the results of Sec. IV are indeed optimal, but our surfaces must eventually enter the vacuum exterior in order to close, and the complications there are such that a full proof escapes us. Section VI contains further discussion about trapped surfaces in the OS spacetime, and asks some questions we would like to see answered. Section VII gives our conclusions.

II. THE OPPENHEIMER-SNYDER SOLUTION

The Oppenheimer-Snyder solution consists of a piece of a $k = 1$ dust-filled Friedmann model, matched across comoving spheres to a timelike hypersurface in the Schwarzschild solution ruled by timelike geodesics [15]. This solution was a midwife for the notion of black holes, and still plays an important role, say, as a model example for numerical relativity [16]. Technicalities apart, it is best explained by a picture. See Fig. 1, whose caption provides a reminder of the salient facts.

The technicalities are important for our purposes though. The metric within the dust cloud is

$$ds^2 = -d\tau^2 + a^2(\tau)[d\chi^2 + \sin^2\chi(d\theta^2 + \sin^2\theta d\phi^2)] = a^2(\eta)[-d\eta^2 + d\chi^2 + \sin^2\chi(d\theta^2 + \sin^2\theta d\phi^2)]. \quad (1)$$

This is a solution of Einstein's equations if

$$a(\eta) = \frac{a_m}{2}(1 - \cos\eta), \quad (2)$$

$$\tau(\eta) = \frac{a_m}{2}(\eta - \sin\eta), \quad (3)$$

where a_m is a constant determining the minimum energy density of the dust cloud. The dust is moving along timelike geodesics at constant χ, θ, ϕ. We assume that we are in the collapsing phase ($\pi < \eta < 2\pi$, $a_{,\tau} < 0$), and moreover less than half of the 3-sphere is included ($\chi \leq \chi_0 < \pi/2$) because we are going to match this solution to Schwarzschild at the comoving hypersurface $\chi = \chi_0 < \pi/2$.

In the exterior we have the Schwarzschild metric

$$ds^2 = -V(r)dt^2 + \frac{dr^2}{V(r)} + r^2(d\theta^2 + \sin^2\theta d\phi^2), \qquad V(r) = 1 - \frac{2M}{r}. \quad (4)$$

We assume that $r \geq a\sin\chi_0$ in order to match the two solutions across the hypersurface,

$$r = R(\eta) = a\sin\chi_0. \quad (5)$$

Equations (2) and (3) are still in force, and imply that this hypersurface is ruled by radially infalling Schwarzschild geodesics.

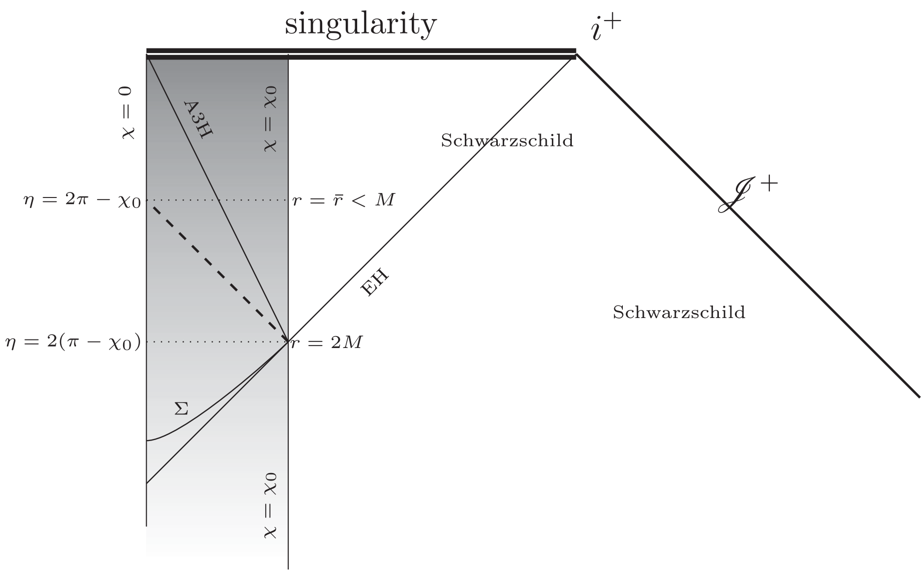

FIG. 1. A Penrose diagram of the OS black hole. The shadowed region is a collapsing part of a closed Friedmann dust model, and the rest is Schwarzschild. The two regions are matched at a comoving timelike hypersurface $\chi = \chi_0$. (The coordinates used are explained in the text.) EH denotes the event horizon, and A3H denotes a timelike tube of marginally trapped surfaces. They meet in a sphere at the junction. The simple argument in Sec. III shows that there are round trapped surfaces above the past light cone defined by the dashed line. Together with EH it defines a causal diamond in which the boundary of the trapped region must lie. The boundary must lie above the hypersurface Σ, which has constant Kodama time and forms a past barrier for trapped surfaces [9]. The interior time at the upper vertex of the diamond defines a round 2-sphere on the matching hypersurface whose area coordinate in the exterior is given by $r = \bar{r} = (M/2)\cos^{-2}(\chi_0/2)$, and this is always less than M, also indicated in the figure.

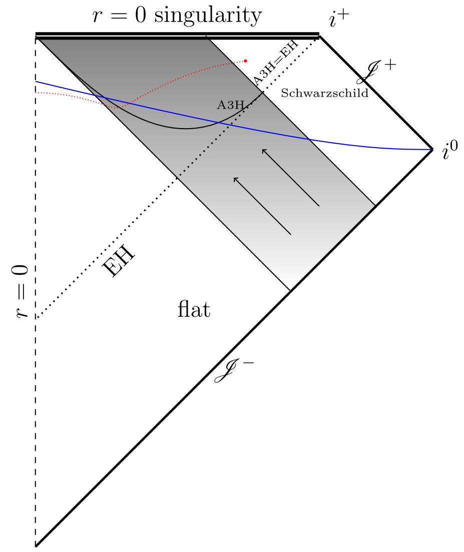

FIG. 2 (color online). A Penrose diagram of a Vaidya solution. The matter region is filled with null dust. Again there is a tube of marginally round trapped spheres within the matter region, but it is a spacelike tube of spheres that cease to be trapped if deformed outwards within suitable hypersurfaces. For instance, the spacelike hypersurface going out to i^0 marked in blue intersects A3H twice, the inner intersection is unstable, while the outer is stable within the given hypersurface. It can be checked that outermost intersections are always stable in this sense. A (nonround) trapped surface going through the center [14] is marked with red dots.

The matching is done in such a way that the first and second fundamental forms of the hypersurface agree, from whatever side they are evaluated. The point of this requirement is to guarantee that there exists a coordinate system (not the ones we are using!) in which the metric is C^1 everywhere. The calculation is well explained in textbooks [17]. It is seen to relate the parameters of the solutions by

$$M = \frac{a_m}{2} \sin^3 \chi_0. \tag{6}$$

This means that the Schwarzschild mass equals the Misner-Sharp mass of the Friedmann model evaluated at the junction hypersurface. Furthermore,

$$t = T(\eta), \qquad T_{,\eta} = \frac{a \cos \chi_0}{V(R)}. \tag{7}$$

Due to translation invariance in the Schwarzschild part t is determined only up to a constant.

As explained in the Appendix, and for the calculations we are going to perform, it is necessary to properly identify the tangent spaces at both sides of the matching hypersurface. First, the unit normal to the matching hypersurface has to be identified with the proper orientation, and this is done simply as

$$n^- = a d\chi \overset{\text{identify}}{\longleftrightarrow} n^+ = \frac{1}{a}(T_{,\eta} dr - R_{,\eta} dt) \tag{8}$$

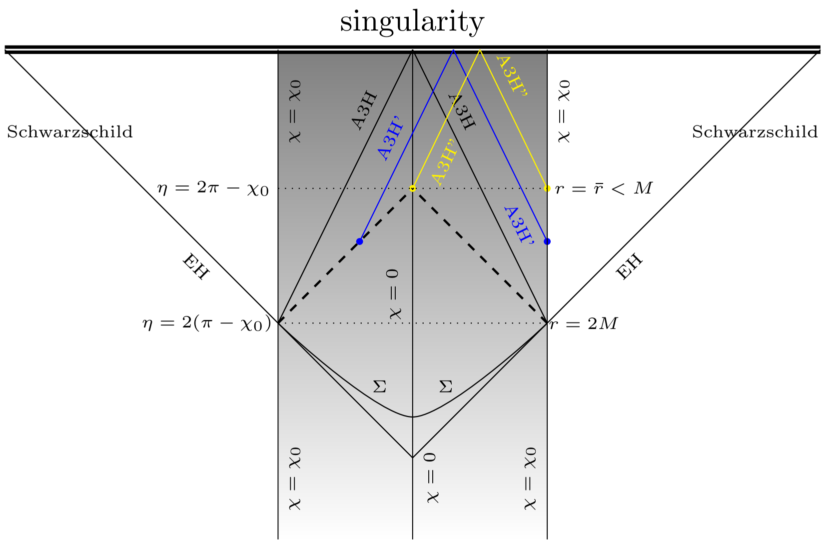

FIG. 3 (color online). A conformal diagram of the OS black hole. Round spheres centered at the origin are represented by two symmetrically placed points, so that the matching hypersurface here is represented by the two vertical lines with constant $\chi = \chi_0$. If the centered round spheres are situated above A3H they are trapped, and they are marginally trapped at A3H itself. However, as the shaded Friedmann region is spatially homogeneous—so that the $\eta =$ constant hypersurfaces (horizontal lines in the shaded part of the diagram) are maximally symmetric—we can move these round spheres, as well as A3H, and center them anywhere on the slices as long as they do not enter the Schwarzschild region. This shows that there are trapped round spheres passing through every point of the interior for all $\eta > 2\pi - \chi_0$. The dashed lines are obtained by shifting the marginally trapped tubes, centering them at values of $\chi \neq 0$, as for example the marginally trapped tube denoted A3H'. The two dots at the end represent a marginally trapped round sphere tangent to the matching hypersurface. The marginally trapped tube denoted A3H'' contains a marginally trapped round sphere—represented by the dots—tangent to both the matching hypersurface and the center at $\eta = 2\pi - \chi_0$.

at $\chi = \chi_0$, where Eqs. (5)–(7) have been used. Then, the tangent vectors have to be identified properly. The angular part is identified in a natural way. Concerning the third tangent vector, we note that there is a uniquely defined timelike unit vector tangent to the matching hypersurface and orthogonal to the round spheres on both sides, and they are naturally identified by

$$e^-_\eta = \frac{1}{a}\partial_\eta \overset{\text{identify}}{\longleftrightarrow} \frac{1}{a}(T_{,\eta}\partial_t + R_{,\eta}\partial_r) \tag{9}$$

at $\chi = \chi_0$, where again Eqs. (5)–(7) must be used.

Finally the tube of marginally trapped round spheres that we mentioned in the Introduction is located at

$$\text{A3H: } a^2_{,\tau} = \cot^2\chi \Rightarrow \eta = 2\pi - 2\chi. \tag{10}$$

Space is collapsing so quickly that any round sphere larger than this is trapped.

There is a past barrier Σ for trapped surfaces [9] defined by the concrete value of "Kodama time" such that the hypersurface Σ meets the event horizon EH at the matching hypersurface $\chi = \chi_0$, which happens at $\eta = 2(\pi - \chi_0)$. In the region below A3H [for $\eta < 2(\pi - \chi)$] of the interior Friedmann part, Kodama time is given by constant values of $\cos^2\frac{\eta}{2}\cos\chi$, and thus

$$\Sigma\text{: } \cos^2\frac{\eta}{2}\cos\chi = \cos^3\chi_0.$$

It is interesting to compare the OS solution to the Vaidya model; see Fig. 2. The latter also has a tube of marginally trapped round spheres, but the Vaidya tube is spacelike, and its marginally trapped spheres are outermost stable, in the sense that if they are deformed outwards within a suitable spacelike hypersurface they cease to be trapped. In the OS model, on the contrary, they cease to be trapped if deformed inwards. In this sense they are unstable [10]. Several studies of nonspherically symmetric trapped surfaces in the Vaidya spacetime are available [7,14,18].

III. TRAPPED SURFACES WITHIN THE DUST CLOUD

Before considering surfaces extending into both the Friedmann and the Schwarzschild region of the OS solution, let us warm up with round spheres contained within the dust cloud. We know that there is a marginally trapped tube (10) consisting of round spheres centered at $\chi = 0$. However, since space is homogeneous, a round sphere within the dust cloud centered at some other value of χ must also be marginally trapped. Thus the marginally trapped round spheres inside the cloud can freely be moved around while still being marginally trapped, as long as they do not extend into the exterior Schwarzschild region.

In the conformal diagram of Fig. 3 the maneuver is illustrated by shifting the marginally trapped tube A3H to the left or right. Every pair of symmetrically placed points on the shifted tube represents a marginally trapped round sphere, as long as both points are contained within the dust cloud. Thus we immediately see that the region above the dashed lines is filled with marginally trapped surfaces.

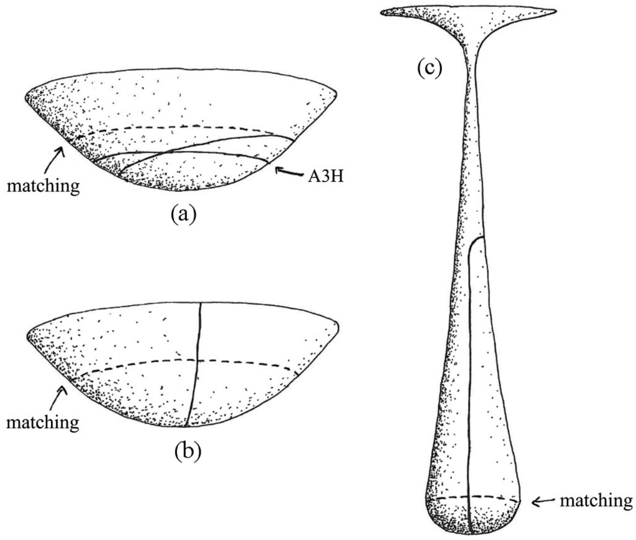

FIG. 4. Three different spatial slices of the OS model embedded in Euclidean space with one dimension suppressed. (a) A constant η hypersurface in Friedmann matched to a spacelike hypersurface in Schwarzschild. Horizontal circles represent round spheres. The dashed circle is the sphere at $\chi = \chi_0$ where the matching is made. The continuous circles are marginally trapped spheres inside the dust cloud. One of them lies on A3H at a constant value of χ. The other one is obtained by tilting the first one until it becomes tangent to the surface of the star. We see that the tilted circle reaches smaller values of χ. (b) The same spatial slice as in (a) with the equatorial plane drawn as a black curve. This surface reaches the center at $\chi = 0$, but it also extends into the Schwarzschild region and it is not clear whether it can be closed or not. (c) The spatial slice on which the surface of Sec. IVA lies. The surface is drawn as a black curve. At a small enough value of r it deviates from the equatorial plane and is closed. Far from the cloud the hypersurface is bent so that it reaches spatial infinity—rather than ending up in the singularity—giving an intuitive definition of an "outer" direction on the surface.

We may also visualize the argument by drawing a picture of a spatial slice with η constant inside the cloud; see Fig. 4. Suppressing one dimension, the dust cloud—which is a part of a 3-sphere—can be drawn as part of a 2-sphere embedded in Euclidean space. Spheres of constant χ on the spatial slice are represented by horizontal circles on the spherical cap in the picture. The shifted spheres are illustrated in the picture by tilting these circles. By taking a circle representing a marginally trapped sphere and tilting it we find that it can reach smaller values of χ than the original one. But for values of η smaller than $2\pi - \chi_0$ the center will not be reached in this way, since that would require extending into the Schwarzschild region.

If we want to find a trapped surface passing through the center at the earliest possible time η it must venture into the exterior. In Fig. 4 we see that we reach smaller values of χ the more we tilt the circles. The smaller the value of η the more we need to tilt the marginally trapped surfaces in order to reach the center. The intuitive strategy for optimizing the problem is thus to consider a circle tilted to the extreme so that it becomes vertical in the picture, i.e. to consider an equatorial plane.

IV. EQUATORIAL SURFACES PASSING THROUGH THE CENTER

We believe that surfaces confined to an equatorial plane have the best chance of reaching the center of the dust cloud at early times, as argued in the previous section. Still, we have to determine the exact shape of the surface in the interior as well as in the exterior, and the two pieces must be matched properly. Throughout we restrict ourselves to axially symmetric surfaces. We believe that allowing for more general surfaces will not improve the results, but we must admit that we do not have a proof of this statement.

The interior as well as the exterior is spherically symmetric, and despite the fact that we should have taken coordinates θ^+, ϕ^+ in the interior and θ^-, ϕ^- in the exterior, by adapting them if necessary we can obviously drop the $\pm$ and take θ and ϕ as coordinates on the round spheres in the whole spacetime, and in particular on the matching hypersurface. Choosing the surface to lie in the equatorial plane $\theta = \pi/2$, we can describe it with local coordinates λ and φ. As mentioned above, we assume that the surface is axially symmetric, and thus we set $\phi = \varphi$ so that on the interior part of the surface $\eta = \eta(\lambda)$ and $\chi = \chi(\lambda)$ are then functions only of λ, and in the exterior $r = r(\lambda)$ and $t = t(\lambda)$ are functions only of λ.

As explained in the Appendix there arise some constraint equations [Eqs. (A2)] to ensure that the surface meets the matching hypersurface at the same set. The first of these constraints is

$$\chi(\lambda) = \chi_0,$$

and we assume that it has a solution given by λ_0. Then the value of η at the intersection of the surface with the matching hypersurface is fixed and given by

$$\eta_0 \equiv \eta(\lambda_0).$$

The constraints involving the exterior part then become

$$T(\eta_0) = t(\lambda_0) \equiv t_0, \qquad R(\eta_0) = r(\lambda_0) \equiv r_0,$$

where t_0 and r_0 denote the values of t and r at the intersection of the surface with the matching hypersurface. The first of these poses no problems due to the freedom in the choice of $T(\eta)$. Concerning the second, it leads to the basic relation

$$r_0 = a(\eta_0)\sin\chi_0 \Leftrightarrow \cos\eta_0 = 1 - \frac{r_0}{M}\sin^2\chi_0, \quad (11)$$

determining the exterior value r_0 in terms of the interior values χ_0 and η_0. It is also possible to think that it determines the relation between η_0 and r_0 given the value of χ_0.

The null normals to the surface, on which the expression for the second fundamental form depend, are given by

$$k^{\pm\mu} = \begin{cases} \frac{1}{a\sqrt{\chi'^2-\eta'^2}}(\chi'\partial_\eta + \eta'\partial_\chi) \pm \frac{1}{a\sin\chi}\partial_\theta & \text{on the Friedmann side,} \\ \frac{1}{\sqrt{\Delta}}\left(\frac{r'}{V}\partial_t + t'V\partial_r\right) \pm \frac{1}{r}\partial_\theta & \text{on the Schwarzschild side,} \end{cases} \quad (12)$$

where the primes denote differentiation with respect to λ. They are normalized such that $k^{\pm\mu}k^{\pm}_{\mu} = -2$. With these null normals the null expansions are

$$\theta^{\pm} = \begin{cases} \frac{1}{2a\sqrt{\chi'^2-\eta'^2}}\left(\frac{\chi'\eta''-\eta'\chi''}{\chi'^2-\eta'^2} + \eta'\cot\chi + 2\chi'\cot\frac{\eta}{2}\right), \\ -\frac{1}{2r\Delta^{3/2}}\left(r\left(r'' - \frac{r'}{t'}t''\right) + \frac{M+r}{2M-r}r'^2 + \frac{1}{r^2}(M-r)(2M-r)t'^2\right), \end{cases} \quad (13)$$

in the Friedmann and Schwarzschild parts, respectively.

The null normals (12) agree on the matching hypersurface [in other words, they comply with the necessary conditions (A4) that can be computed using Eqs. (8) and (9)] if the following holds:

$$\chi'(\lambda_0) = \frac{1}{a^2}(r'T_{,\eta} - t'R_{,\eta})|_{\lambda_0}, \quad (14)$$

$$\eta'(\lambda_0) = \frac{1}{a^2 V}(t'V^2T_{,\eta} - r'R_{,\eta})|_{\lambda_0}, \quad (15)$$

where Eq. (11) has been taken into account. This fixes the first derivatives of $\chi(\lambda)$ and $\eta(\lambda)$ at λ_0 given those of $r(\lambda)$ and $t(\lambda)$ there. An equivalent version, interchanging both sides, reads

$$r'(\lambda_0) = (\chi'VT_{,\eta} + \eta'R_{,\eta})|_{\lambda_0}, \quad (16)$$

$$t'(\lambda_0) = \frac{1}{V}(\chi' R_{,\eta} + \eta' V T_{,\eta})|_{\lambda_0}, \tag{17}$$

and can be obtained by solving Eqs. (14) and (15) as equations for $r'(\lambda_0)$ and $t'(\lambda_0)$.

We may now compute the first and second fundamental forms of the surface. The results are presented in Table I. The Δ appearing in the table is defined as

$$\Delta = \frac{r'^2}{V} - t'^2 V. \tag{18}$$

It has to be positive for the surface to be spacelike.

All the things listed in Table I must be continuous across the matching hypersurface, as explained in more detail in the Appendix. The continuity of the third fundamental form—which is not listed in the table—trivially holds since it vanishes on both sides of the matching hypersurface. Some of the continuity conditions of Table I are already fulfilled due to Eq. (11) and either of Eqs. (14) and (15) or Eqs. (16) and (17). The rest yields the remaining matching conditions for the surface, fixing the second derivatives as

$$\chi''(\lambda_0) = \left(\chi' \frac{\partial_\lambda \gamma_{\lambda\lambda}}{2\Delta} + \eta' \frac{K_{\lambda\lambda}}{\sqrt{\Delta}} - 2\frac{R_{,\eta}}{r}\chi'\eta'\right)\Bigg|_{\lambda_0}, \tag{19}$$

$$\eta''(\lambda_0) = \left(\eta' \frac{\partial_\lambda \gamma_{\lambda\lambda}}{2\Delta} + \chi' \frac{K_{\lambda\lambda}}{\sqrt{\Delta}} - \frac{R_{,\eta}}{r}(\chi'^2 + \eta'^2)\right)\Bigg|_{\lambda_0}, \tag{20}$$

where the values of $\partial_\lambda \gamma_{\lambda\lambda}$ and $K_{\lambda\lambda}$ are the expressions given in Table I on the Schwarzschild side evaluated at the matching hypersurface. As before, we can also write these conditions in an alternative way by interchanging the roles of both sides as

$$r''(\lambda_0) = \left(r' \frac{\partial_\lambda \gamma_{\lambda\lambda}}{2\Delta} + t' V \frac{K_{\lambda\lambda}}{\sqrt{\Delta}} + \frac{M}{r^2}\Delta\right)\Bigg|_{\lambda_0}, \tag{21}$$

$$t''(\lambda_0) = \left(t' \frac{\partial_\lambda \gamma_{\lambda\lambda}}{2\Delta} + \frac{r'}{V}\frac{K_{\lambda\lambda}}{\sqrt{\Delta}} - \frac{2M}{r^2}\frac{r't'}{V}\right)\Bigg|_{\lambda_0}, \tag{22}$$

where $\partial_\lambda \gamma_{\lambda\lambda}$ and $K_{\lambda\lambda}$ are now evaluated at the matching hypersurface using the expressions on the Friedmann side.

In the rest of this section we will present two different choices for the functions of λ describing the surface. In the first example the surface will be specified in Schwarzschild, putting restrictions on the values of the functions $\eta(\lambda)$ and $\chi(\lambda)$ and their first and second derivatives at the junction. In our second example the surface will be specified in the Friedmann part, putting restrictions on how it can be continued into Schwarzschild.

A. The first construction

In this section we make a simple ansatz for the surface and optimize that particular construction. This will then give us a hint of what the truly optimized solution might be.

We have already decided on sticking to the equatorial plane close to the center of the cloud. However, the surface must eventually leave the equatorial plane in order to be closed. It has been shown [14] that an equatorial surface of constant r within the Schwarzschild part can be closed properly—that is, being closed while held trapped—if the constant value of r is small enough. Even though we want to keep things simple we have a better chance of succeeding in our quest if we add one degree of freedom, letting not r be constant but rather $dr/dt = r'/t' = k$ with k constant. A small enough value of r can always be reached if k is negative. Once this value has been reached the surface can be bent into a surface of constant r by letting $d^2r/dt^2 = (r'' - (r'/t')t'')/t'^2$ differ from zero in a small region. This is harmless, since we see from Eq. (13) that a positive $r'' - (r'/t')t''$ will only make the null expansions more negative.

Demanding that the surface is spacelike and that the null expansions are nonpositive will put restrictions on the constant k. The surface is spacelike if the Δ of Eq. (18) is positive everywhere. We want to keep the surface inside the event horizon, so the function $V(r)$ is negative, and thus the condition becomes that $k > V$ everywhere. The function $V(r)$ obtains its maximum value when r does, which by construction is at the junction. Thus the lower bound for k is given by

TABLE I. The nonvanishing components of the first fundamental form γ_{AB} and its derivatives and the second fundamental form K_{AB} in the interior and the exterior for a surface in the equatorial plane. The primes indicate differentiation with respect to λ.

	Friedmann	Schwarzschild
$\gamma_{\lambda\lambda}$	$a^2(\chi'^2 - \eta'^2)$	Δ
$\gamma_{\varphi\varphi}$	$a^2\sin^2\chi$	r^2
$\partial_\lambda\gamma_{\lambda\lambda}$	$2a^2(\chi'\chi'' - \eta'\eta'' + a_{,\tau}\eta'(\chi'^2 - \eta'^2))$	$2(\frac{r'r''}{V} - t't''V - \frac{r'}{V}\frac{M}{r^2}(\frac{r'^2}{V} + t'^2V))$
$\partial_\lambda\gamma_{\varphi\varphi}$	$2a^2\sin^2\chi(a_{,\tau}\eta' + \chi'\cot\chi)$	$2rr'$
$K_{\lambda\lambda}$	$\frac{a}{\sqrt{\chi'^2-\eta'^2}}(\chi'\eta'' - \eta'\chi'' + a_{,\tau}\chi'(\chi'^2 - \eta'^2))$	$\frac{1}{\sqrt{\Delta}}(r't'' - t'r'' + t'\frac{M}{r^2}(\frac{3r'^2}{V} - t'^2V))$
$K_{\varphi\varphi}$	$\frac{a\sin^2\chi}{\sqrt{\chi'^2-\eta'^2}}(a_{,\tau}\chi' + \eta'\cot\chi)$	$\frac{1}{\sqrt{\Delta}}rt'V$

$$k > 1 - \frac{2M}{r_0}. \tag{23}$$

With our choice $r'(\lambda) = kt'(\lambda)$ the null expansions in Eq. (13) are nonpositive if

$$k^2 \geq \frac{r - M}{r + M} V^2. \tag{24}$$

There are now three different cases. If r_0—and thus every other value of r on the exterior part of the surface—is less than M, the surface is safely trapped in the exterior. The right-hand side of Eq. (24) attains its maximum when

$$r = r_m = \frac{M}{3}(1 + \sqrt{7}) \approx 1.22M.$$

If r_0 is less than this value it is enough to check that the null expansions are nonpositive at the junction, and if it is larger than this value it is enough to check that the null expansions are nonpositive at $r = r_m$. We get the following upper bounds for k:

$$k \leq \begin{cases} 0 & \text{if } r_0 \leq M, \\ \left(1 - \frac{2M}{r_0}\right)\sqrt{\frac{r_0 - M}{r_0 + M}} & \text{if } M \leq r_0 \leq r_m, \\ \left(1 - \frac{2M}{r_m}\right)\sqrt{\frac{r_m - M}{r_m + M}} & \text{if } r_0 \geq r_m. \end{cases} \tag{25}$$

There is also an upper bound for r_0. When

$$r_0 = 2M\left(1 - \left(1 - \frac{2M}{r_m}\right)\sqrt{\frac{r_m - M}{r_m + M}}\right)^{-1} = \frac{2M}{1 + \sqrt{14\sqrt{7} - 37}} \approx 1.66M \tag{26}$$

the lower and the upper bounds for k become equal, leaving only one choice for k. If r_0 is larger than this value the surface cannot be both spacelike and trapped. Observe that there is plenty of room between the value $r = \bar{r} = \frac{M}{2\cos^2\frac{\chi_0}{2}} < M$ shown in Fig. 1 and this value where our surface can intersect the matching hypersurface.

The surface in the exterior is now specified by choosing a value of r_0 less than the value (26), and a value of k satisfying the conditions (23) and (25) given r_0. It must then be matched to a surface in the interior. Suppose that the equatorial surface in the interior is determined by a function f such that $\eta = f(\chi)$. This function must satisfy

$$f(\chi_0) = \eta_0,$$

with η_0 given by the matching condition (11). The values of the first and second derivatives of f,

$$\frac{df}{d\chi} = \frac{\eta'(\lambda)}{\chi'(\lambda)}, \qquad \frac{d^2 f}{d\chi^2} = \frac{1}{\chi'^2(\lambda)}\left(\eta''(\lambda) - \chi''(\lambda)\frac{\eta'(\lambda)}{\chi'(\lambda)}\right),$$

are determined at the junction by the matching conditions (14), (15), (19), and (20). If we make the simple ansatz

$$f(\chi) = k_0 + k_1\chi^2 + k_2\chi^4, \tag{27}$$

the coefficients k_0, k_1 and k_2 are completely determined by the matching conditions.

The null expansions for the surface in the interior are given by Eq. (13). We want to choose r_0 and k so that the coefficient k_0 of Eq. (27)—that is, the value of η at which the surface reaches the center of the cloud—is as small as possible while the null expansions are still nonpositive. From Fig. 5 we conclude that the best we can do is to choose the two constants r_0 and k so that the surface is

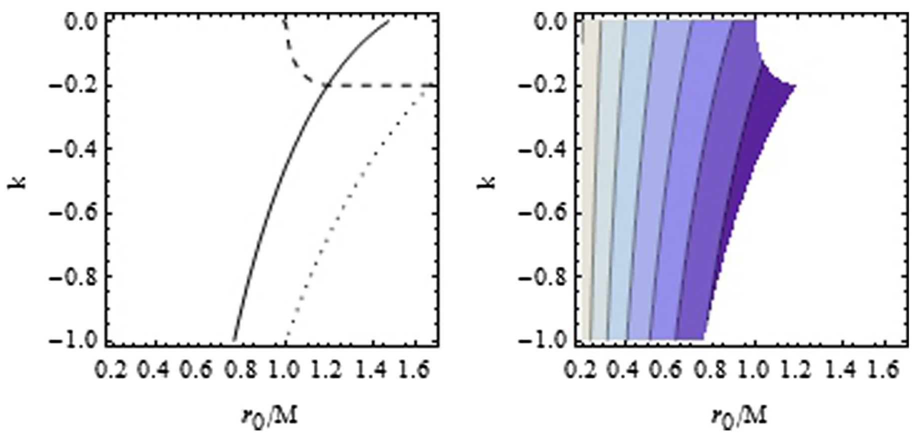

FIG. 5 (color online). The plots show how to choose r_0 and k so that the value of k_0 becomes the smallest possible when $\chi_0 = \pi/4$. The plot to the left helps us identify the allowed choices. Above the dotted curve the condition (23) holds and the surface is spacelike. Below the dashed curve k satisfies the inequality (25), with equality on the curve, and the surface is trapped in the exterior. To the left of the continuous curve the surface is trapped at the center $\chi = 0$, and on the curve it is marginally trapped there. We conclude that the allowed region cannot extend past the continuous and dashed curves to the right. The contour plot to the right shows the value of k_0 with the forbidden (white) region excluded. The darker the shade, the smaller the value of k_0. We see that the best choice of r_0 and k is the values they take where the continuous and the dashed curves intersect.

TABLE II. The smallest values of η at the center for the two constructions at different values of χ_0. The first construction gives an optimal solution and the result is given to five-digit accuracy. In the second construction the values are the smallest possible to three-digit accuracy so that the surface becomes well behaved in the exterior. The smaller the dimensionless number X, the sooner the surfaces meet the center compared to a given reference time.

	χ_0	$\pi/12$	$\pi/6$	$\pi/4$	$\pi/3$	$5\pi/12$
First construction	$\eta(0)$	5.7693	5.2716	4.8037	4.3752	4.0081
	X	0.037005	0.067999	0.11628	0.17797	0.26197
Second construction	$\eta(0)$	5.77	5.26	4.79	4.36	4.00
	X	0.040	0.046	0.099	0.16	0.26

marginally trapped at the center and so that it is either marginally trapped at the junction, if $r_0 < r_m$, or marginally trapped at $r = r_m$, if $r_0 > r_m$. The plots in Fig. 5 are for $\chi_0 = \pi/4$, but similar analyses for four other values of χ_0 confirm the result. It may also be confirmed that with this choice of r_0 and k the null expansions are negative for all values of χ between 0 and χ_0 in the studied cases. The results for k_0 are shown in Table II. In Fig. 6 the location of the best surface in a Penrose diagram of the Friedmann portion is shown for a few different values of χ_0. A complete Penrose diagram, with the entire construction of the surface both in the interior and the exterior, is presented in Fig. 7. Yet another picture of the surface for $\chi_0 = \pi/4$—here embedded in Euclidean space—is shown in Fig. 4.

B. The second construction

In the previous construction we found that the optimal choice of the surface was such that it was marginally trapped at some critical points. The result can be made slightly better by choosing the surface so that it is kept marginally trapped everywhere inside the dust cloud and then matching it to some suitable surface in the exterior.

We want the surface to reach the center $\chi = 0$, and we also keep it in an equatorial plane with axial symmetry; hence, it lies on a spacelike spherically symmetric hypersurface. There is a general result [19] that implies that then the surface cannot be (marginally) trapped at any local maximum of χ in the region below A3H. Thus, we can safely choose $\chi(\lambda) = \lambda$ so that the null expansions (13) in the interior become

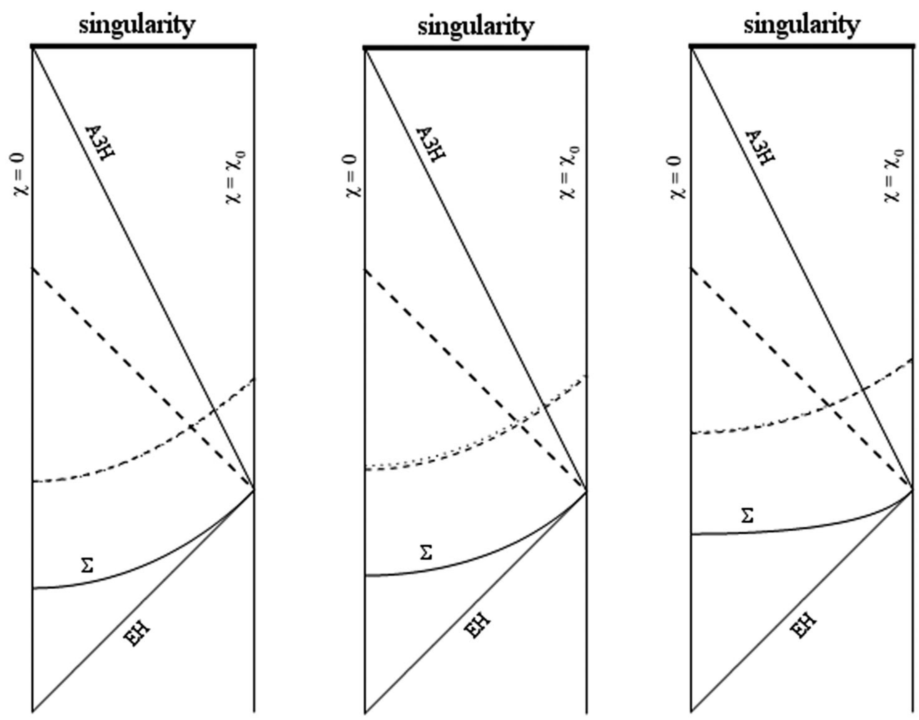

FIG. 6. Penrose diagrams of the interior of the dust cloud with $\chi_0 = \pi/12$, $\chi_0 = \pi/4$ and $\chi_0 = 5\pi/12$ from left to right. The dotted curves represent the best surfaces we get in the first construction. A point on each curve really represents a sphere in the Penrose diagram, but only the equator of each such sphere is part of the surface. The dashed curves represent the marginally trapped surfaces in the second construction. The two results are barely distinguishable to the eye in this figure.

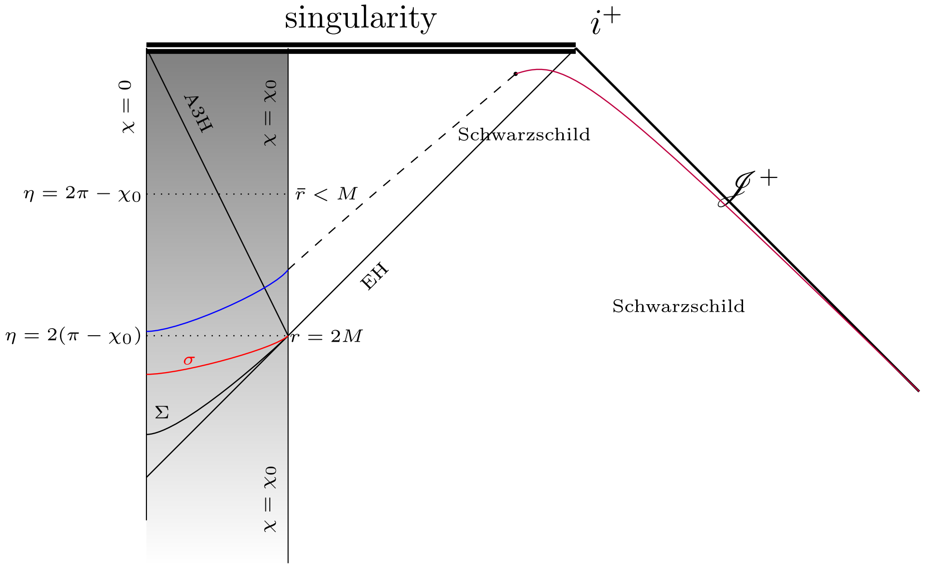

FIG. 7 (color online). The OS black hole once again, with some novel decoration. The equatorial planes of the blue hypersurface can be joined to appropriate cylinders in the Schwarzschild region—represented here by the dashed line—such that they can eventually be capped (the final dot) to produce topological spheres that are (weakly) trapped, as has been explicitly demonstrated in the main text. The purple line together with the dashed and blue lines indicates how a possible spacelike and asymptotically flat hypersurface containing the trapped surface looks in the diagram. This hypersurface corresponds to the spatial slice shown in Fig. 4(c). The particular hypersurface called σ shown in red has minimal equatorial planes and joins the past barrier Σ and the EH at the round 2-sphere with $\chi = \chi_0$ and $\eta = 2(\pi - \chi_0)$, as represented. In the main text we prove that σ is a past barrier for axially symmetric trapped surfaces which are confined to equatorial planes within the interior part. One wonders if σ can be promoted to a new past barrier for more general trapped surfaces, leaving even less room for the boundary $\mathcal{B}$ to be placed.

$$\theta_{\pm} = \frac{1}{2a\sqrt{1-\eta'^2}}\left(\frac{\eta''}{1-\eta'^2} + \eta' \cot\chi + 2\cot\frac{\eta}{2}\right). \tag{28}$$

Putting these to zero gives a differential equation for $\eta(\lambda)$. If we give as initial conditions the value $\eta(0)$ at the center and demand $\eta'(0) = 0$ this differential equation can be solved numerically. This will completely determine the surface in the interior.

We must then make an ansatz for the surface in the exterior. Suppose that the surface lies in the equatorial plane with $r = g(t)$ for some function g. Let us set the value of t at the junction to zero: $t_0 = t(\lambda_0) = 0$. Then we must have that $g(0) = r_0$ with the value of r_0 determined by the matching condition (11). The first and second derivatives of g are

$$\frac{dg}{dt} = \frac{r'(\lambda)}{t'(\lambda)}, \qquad \frac{d^2g}{dt^2} = \frac{1}{t'^2(\lambda)}\left(r''(\lambda) - t''(\lambda)\frac{r'(\lambda)}{t'(\lambda)}\right),$$

and their values at $\lambda_0 \Leftrightarrow t = 0$ are determined by the matching conditions (16), (17), (21), and (22). A simple ansatz for g is to put

$$g(t) = g(0) + g'(0)t + \frac{1}{2}g''(0)t^2.$$

The whole construction is then completely determined by the value we choose for $\eta(0)$.

We want to choose $\eta(0)$ as small as possible but need to make sure that the chosen value makes the function $g(t)$ well behaved in the exterior—meaning that the surface can be closed and that the null expansions are negative. We do not give an explicit description of how the surface is to be closed in Schwarzschild, but we know that as long as small enough values of r can be reached it can be done [14]. The values of $\eta(0)$ presented in Table II are such that the function $g(t)$ reaches values at least smaller than $0.02M$, and such that the null expansions are negative in the exterior. The result is drawn next to the surface resulting from the first construction in the Penrose diagrams of Fig. 6 for three different values of χ_0. It is striking how close the two results are to each other.

The value of $\eta(0)$ for the optimal trapped surface depends on the value of χ_0 as we can check in Table II. To compare these different values, in order to see how the trapped surfaces extend to the center depending on the physical parameters of the black hole, we take as the reference time for all possible black holes $\eta = 2(\pi - \chi_0)$, that is, the first instant in η with a marginally trapped round sphere. We want to compute how close to this reference time the trapped surfaces we have constructed can be. To that end, we define the dimensionless number

$$X \equiv \frac{\eta(0) - 2(\pi - \chi_0)}{\chi_0},$$

and the smaller its value, the sooner the trapped surfaces are met at the center of the dust cloud. These values are presented for both constructions in Table II. The second construction is better than the first in all cases except for the case $\chi_0 = \pi/12$. For the latter case a more accurate analysis of the second construction would be needed to detect any difference. Not taking the smallest value of χ_0 into consideration, we can check that X is an increasing function of χ_0. We draw the conclusion that the smaller the value of χ_0, or in physical terms the smaller the mass M of the black hole for a fixed energy density of the cloud, the sooner the trapped surfaces reach the center of the cloud with respect to the reference time. Another way of putting this is: the comoving time η elapsed between the first appearance of a marginally trapped round sphere and that of a trapped surface reaching the center increases with the mass of the OS black hole (for a fixed energy density of the dust).

V. THE OPTIMAL CONSTRUCTION?

In this section we discuss whether the construction in Sec. IV is optimal or not. There are some general results we can reach by considering only the Friedmann part of the surface, but still it must be admitted that the final result is dependent on the closing of the surface in Schwarzschild. The surfaces constructed in Sec. IV B are minimal inside the dust cloud. We will here prove that any minimal surface in the equatorial plane within the dust cloud reaches values of η at the center that are lower than those reached by any other possible axially symmetric trapped surface crossing any round sphere intersected by the former in the interior region. We do this in three steps: first we consider minimal surfaces and show that, for MTSs on equatorial planes, η is an increasing function of χ everywhere in the dust cloud; second, we prove that the claim holds for axially symmetric surfaces restricted to an equatorial plane; finally, we remove the equatorial-plane condition.

A. Minimal equatorial planes

Let us start by proving that any (piece of a) minimal surface cannot have a local maximum of η within the Friedmann part of the spacetime. For a two-dimensional surface S with tangent vectors $\vec{e}_A$ and mean curvature vector $\vec{H}$ the following relation holds [9]:

$$\frac{1}{2}\gamma^{AB}e^{\mu}_{A}e^{\nu}_{B}(\mathcal{L}_{\vec{\xi}}g|_S)_{\mu\nu} = \bar{\nabla}_C\bar{\xi}^C + \xi_\alpha H^\alpha, \tag{29}$$

for any vector field $\vec{\xi}$. In Eq. (29) $\bar{\nabla}_A$ is the Levi-Civita connection of the first fundamental form γ_{AB}, i.e. $\bar{\nabla}_A\gamma_{BC} = 0$, and $\bar{\xi}_A$ is the projection of $\vec{\xi}$ on the surface, that is, $\bar{\xi}_A = \xi_\mu|_S e^{\mu}_{A}$. Let us choose $\vec{\xi} = \partial_\eta$, which is a future-pointing, timelike, conformal Killing vector field orthogonal to the spacelike hypersurfaces of constant η. Then

$$(\mathcal{L}_{\vec{\xi}}g)_{\mu\nu} = 2a_{,\tau}g_{\mu\nu},$$

and

$$\bar{\xi}_A = \xi_\mu e^{\mu}_{A} = -a^2\bar{\nabla}_A\eta.$$

If the surface is minimal $\vec{H} = \vec{0}$, and we find that with our choice of $\vec{\xi}$ Eq. (29) becomes

$$2a_{,\tau} = -a^2(\bar{\nabla}_A\bar{\nabla}^A\eta + 2a_{,\tau}\bar{\nabla}_A\eta\bar{\nabla}^A\eta). \tag{30}$$

At a local extremum $q \in S$ of η we have that $\bar{\nabla}_A\eta|_q = 0$, so Eq. (30) becomes

$$\bar{\nabla}_A\bar{\nabla}^A\eta|_q = -2\frac{a_{,\tau}}{a^2}\bigg|_q > 0.$$

The right-hand side of this equation is positive and thus any local extremum of η must be a minimum. This applies, in particular, to axially symmetric marginally trapped surfaces confined to an equatorial plane because, as we know from Eq. (13), both expansions are equal and thus any MTS is actually minimal there.

There are also some conclusions we can draw on the behavior of trapped and marginally trapped surfaces at the center. Consider an axially symmetric surface in an equatorial plane and, as in Sec. IV B, let us choose the parameter λ on the surface so that $\chi(\lambda) = \lambda$, $0 \le \lambda \le \chi_0$. The null expansions are then given by Eq. (28). We see that any surface must have a local extremum at the center,

$$\eta'(0) = 0, \tag{31}$$

or otherwise the second term of Eq. (28) diverges. Then we have that

$$\lim_{\lambda\to 0}\frac{\eta'(\lambda)}{\tan\lambda} = \lim_{\lambda\to 0}\frac{\eta''(\lambda)}{1+\tan^2\lambda} = \eta''(0),$$

so that the null expansions at the center are

$$(a\theta_\pm)|_{\lambda=0} = 2\left(\eta''(0) + \cot\frac{\eta(0)}{2}\right). \tag{32}$$

They are nonpositive if

$$\eta''(0) \le -\cot\frac{\eta(0)}{2}\,(>0). \tag{33}$$

We see that for a trapped surface this local extremum can be either a minimum or a maximum. But for a marginally trapped (ergo minimal) surface the equality sign of Eq. (33) holds, and the surface must have a minimum at the center.

From the results so far we can draw the conclusion that for an axially symmetric marginally trapped (ergo minimal) surface in an equatorial plane the function $\eta(\lambda)$ has a local minimum at the center and—since it cannot have a maximum—is everywhere an increasing function of λ. Since Eq. (31) holds for trapped as well as minimal surfaces at the center, they are tangent there. Also we see from

Eq. (33) that the value of the second derivative of $\eta(\lambda)$ at the center for any trapped surface is smaller than the corresponding value for a minimal surface. Thus an axially symmetric trapped surface in an equatorial plane is, close to the center, locally to the past of the minimal equatorial plane passing through the center at the same instant of time.

B. Axially symmetric trapped surfaces on equatorial planes

We will now give a definite proof that a minimal equatorial plane reaches the center at an earlier time than any other axially symmetric trapped surface on an equatorial plane that happens to cross any round sphere touched by the minimal one. In Sec. IV B we found the minimal equatorial planes by solving the differential equation obtained by putting Eq. (28) to zero, with the initial conditions $\eta(0) = \alpha$, $\eta'(0) = 0$. Let us denote the solution by $\eta_m(\lambda;\alpha)$. For each value of α there is a spacelike hypersurface $\eta = \eta_m(\lambda;\alpha)$ whose equatorial plane is a minimal surface, and the set of all these hypersurfaces defines a foliation of spacetime. We can define a time coordinate $T(\alpha)$ which is constant on each of these hypersurfaces. There is then a function $p(\lambda;\alpha)$ such that for each value of T the hypersurface is defined by

$$\eta - p(\lambda;\alpha) = T(\alpha).$$

It is related to $\eta_m(\lambda;\alpha)$, also defining the foliation, by

$$p(\lambda;\alpha) = \eta_m(\lambda;\alpha) - T(\alpha). \tag{34}$$

We do not have an explicit expression for either $\eta_m(\lambda;\alpha)$ or $T(\alpha)$, and hence not for $p(\lambda;\alpha)$. However, this will not be needed for the proof. Note though that Eq. (34) implies that

$$p'(\lambda;\alpha) = \eta_m'(\lambda;\alpha). \tag{35}$$

A vector field normal to the hypersurfaces is proportional to

$$\vec{v} = \partial_\eta + p'\partial_\chi. \tag{36}$$

Our purpose is to show that any axially symmetric trapped surface in an equatorial plane cannot have a minimum in T. Then, it is clear that such a trapped surface must reach the center at a later time T—that is, at a larger value of η—than any minimal equatorial plane it crosses, since minimal surfaces lie on hypersurfaces of constant T.

The proof is as follows. Consider a surface in the equatorial plane having a minimum in T at a point q. Since the future-directed vector $\vec{v}$ is orthogonal to hypersurfaces of constant T we have $v_a = -h\nabla_a T$ for some function $h > 0$, or projected to the surface

$$\bar{v}_A = -h\bar{\nabla}_A T. \tag{37}$$

If the surface has a local extremum of T at q, then $\vec{v}$ is normal to the surface at that point. Thus

$$\bar{v}_A|_q = 0, \tag{38}$$

implying that $\bar{\nabla}_A T|_q = 0$. Then from Eq. (37) we see that the divergence of $\bar{v}_A$ at q becomes

$$\bar{\nabla}^A\bar{v}_A|_q = -h\bar{\nabla}^A\bar{\nabla}_A T|_q.$$

If the surface has a minimum of T at q, then $\bar{\nabla}^A\bar{\nabla}_A T|_q > 0$, implying that

$$\bar{\nabla}^A\bar{v}_A|_q < 0. \tag{39}$$

We now show that for an axially symmetric surface S in the equatorial plane Eq. (39) is not consistent with the surface being trapped. On S we set $\chi(\lambda) = \lambda$ so that the first fundamental form of the surface is

$$\gamma_{AB}d\lambda^A d\lambda^B = a^2[(1-\eta'^2)d\lambda^2 + \sin^2\lambda d\varphi^2],$$

and it has a timelike normal vector orthogonal to the round spheres of constant η and χ given by $\partial_\eta + \eta'\partial_\chi$. If S has a minimum of T at the point q the vector (36) is normal to the surface at that point implying that

$$\eta'(\lambda)|_q = p'(\lambda;\alpha_0)|_q, \tag{40}$$

with α_0 given by

$$\eta(\lambda)|_q = \eta_m(\lambda;\alpha_0)|_q. \tag{41}$$

The projection of $\vec{v}$ to the surface is

$$\bar{v}_A = a^2|_S(-\bar{\nabla}_A\eta(\lambda) + p'(\lambda;\alpha)\bar{\nabla}_A\chi(\lambda)).$$

Since Eq. (38) holds, the divergence of $\bar{v}_A$ becomes

$$\begin{aligned}\bar{\nabla}^A\bar{v}_A|_q &= a^2(-\bar{\nabla}^A\bar{\nabla}_A\eta(\lambda) + p'(\lambda;\alpha_0)\bar{\nabla}^A\bar{\nabla}_A\chi(\lambda) \\ &\quad + p''(\lambda;\alpha_0)\gamma^{\lambda\lambda})|_q \\ &= \frac{p''(\lambda;\alpha_0) - \eta''(\lambda)}{1-\eta'^2(\lambda)}\bigg|_q,\end{aligned}$$

where Eq. (40) has been used in the last step. With the point q being a local minimum of T, this quantity must be negative according to Eq. (39), so that

$$p''(\lambda;\alpha_0)|_q < \eta''(\lambda)|_q. \tag{42}$$

The null expansions of the surface are given by Eq. (28). Using Eqs. (35), (40), and (41), and the definition of the function η_m, we find that

$$\theta_\pm|_q = \frac{\eta'' - p''}{2a(1-\eta_m'^2)^{3/2}}\bigg|_q.$$

But if the inequality (42) holds, the null expansions are positive and the surface is not trapped at q.

Thus we draw the conclusion that if we only consider axially symmetric surfaces in the equatorial plane, then minimal surfaces reach the center at the earliest possible times. This result supports the statement that the surfaces of Sec. IV are the best we can do.

C. General axially symmetric trapped surfaces

Consider finally any axially symmetric surface S within the dust cloud. They can be described by the following parametric expressions:

$$\eta = \eta(\lambda), \qquad \chi = \chi(\lambda), \qquad \theta = \theta(\lambda), \qquad \phi = \varphi,$$

where $\{\lambda^B\} = \{\lambda, \varphi\}$ are local coordinates on S. The tangent vectors are

$$\vec{e}_\lambda = \eta' \partial_\eta + \chi' \partial_\chi + \theta' \partial_\theta, \qquad \vec{e}_\varphi = \partial_\phi.$$

The first fundamental form reads

$$\gamma_{AB} d\lambda^A d\lambda^B = a^2(\Delta_F^2 d\lambda^2 + \sin^2\chi(\lambda)\sin^2\theta(\lambda) d\varphi^2), \quad (43)$$

with $\Delta_F^2 = \chi'^2 - \eta'^2 + \theta'^2 \sin^2\chi(\lambda) > 0$. The future-pointing null normals can be chosen to be

$$k^\pm_\mu dx^\mu = \frac{a}{\Delta_F}[-\delta^2 d\eta + (\eta'\chi' \pm \theta'\Delta_F \sin\chi) d\chi + (\eta'\theta' \sin\chi \mp \chi'\Delta_F) \sin\chi d\theta],$$

and they satisfy $k^{+\mu} k^-_\mu = -2\delta^2$, with

$$\delta^2 = \chi'^2 + \theta'^2 \sin^2\chi(\lambda) > 0.$$

Then, a somewhat lengthy but straightforward calculation produces the null expansions,

$$\theta^\pm = \frac{1}{a\Delta_F}\Big\{ 2\delta^2 \cot\frac{\eta}{2} + \frac{1}{\Delta_F^2}[\delta^2\eta'' - \eta'\chi'\chi'' + (\chi'^2 - \eta'^2)\chi'\eta'\cot\chi - \eta'\theta'\theta''\sin^2\chi] + \eta'\theta'\cot\theta \pm \frac{1}{\Delta_F}\Big[\sin\chi(\chi'\theta'' - \theta'\chi'') + \theta'\cos\chi(\Delta_F^2 + \delta^2 + \chi'^2) - \Delta_F^2 \chi' \frac{\cot\theta}{\sin\chi}\Big]\Big\}. \quad (44)$$

Assume that S reaches the center $\chi = 0$, and set $\chi(0) = 0$, i.e. $\lambda = 0$ at the center. The last summand in Eq. (44) remains finite only if $\cot\theta(0) = 0$ implying that, at the center, $\theta(0) = \pi/2$. [Observe that the term with $\cot\chi(0)$ cannot compensate for any divergence in $\cot\theta(0)/\sin\chi(0)$ for *both signs*.] The other critical term at the center behaves like $\chi'(0)\eta'(0)\cot\chi(0)$ and this necessarily requires that $\eta'(0) = 0$. [$\chi'(0) = 0$ is not possible as this would make the divergences even worse and would also violate the condition $\Delta_F^2 > 0$.]

All in all, we can set around the center $\chi = \lambda$ and the null expansions (44) become at the center, by taking the appropriate limits,

$$\theta^\pm(0) = \frac{1}{a}\Big(2\eta''(0) + 2\cot\frac{\eta(0)}{2} \pm 4\theta'(0)\Big),$$

and this can be rewritten as

$$\theta^\pm(0) = \Theta \pm \frac{4}{a}\theta'(0),$$

where Θ is the value (32) of the null expansions at the center for another surface $\tilde{S}$ on an equatorial plane *with the same* $\eta(\lambda)$. If S is (marginally) trapped at the center $\theta^\pm(0) \le 0$ for both signs, and thus it is necessary that $\Theta \le 0$, that is, equality can only occur if $\theta'(0) = 0$. This means that $\tilde{S}$ is (marginally) trapped at the center, and hence we know from the result in the previous subsection that $\tilde{S}$ reaches the center at a later or equal time (i.e. at larger or equal values of η) than the minimal equatorial plane passing through the same round sphere as $\tilde{S}$. But then, so does S, which has the same $\eta(\lambda)$.

Thus, we have proven that general axially symmetric surfaces within the interior region reach the center at later times than the equatorial minimal planes. Of course, the entire discussion has been restricted to the interior Friedmann region, and thus one can still wonder if there exist alternative strategies leading to better values of $\eta(0)$. Recall that what prevented us from pushing the surfaces of Sec. IV B further down was that we had to make sure that they could be closed properly. But we do not know any optimal strategy of closing the surfaces, and are therefore unable to prove that they cannot be pushed even further down.

A consequence of the results of this section is that we can define a past barrier for axially symmetric trapped surfaces reaching the center. It is the hypersurface of constant T that meets the event horizon at the junction between Friedmann and Schwarzschild, as shown in Fig. 7. We call this hypersurface σ in analogy with the past barrier Σ of Fig. 1. However, we do not know if σ really is a past barrier for arbitrary trapped surfaces, while Σ certainly is.

VI. DISCUSSION

In the OS model the boundary $\mathcal{B}$ of the trapped region must be a spherically symmetric hypersurface [9] meeting the event horizon at the junction between dust and vacuum. We believe that the results of the previous sections are enough to pinpoint where $\mathcal{B}$ meets the central world line, and they are certainly consistent with $\mathcal{B}$ being spacelike throughout the dust cloud. Can we say more?

We have just a few thoughts to offer concerning this question. It should be possible to say something about what $\mathcal{B}$ looks like very close to the junction hypersurface, or at least whether it is spacelike there. The answer will be decided by trapped surfaces extending partly into the Schwarzschild region. A simple observation we can make is that the round trapped surfaces inside Schwarzschild can also be "tilted" to a considerable extent very close to the event horizon and still remain trapped. Thus, consider topological spheres at constant r defined by

$$r = r_0, \qquad t = cr_0 \cos\theta, \quad (45)$$

where c is a constant. Their intrinsic geometry is that defined by the intersection of a cylinder with a tilted plane. The point we wish to make is that these surfaces are trapped for all values of $c < 1$, independently of the value of $r_0 < 2M$. If the junction to the dust cloud is placed at some $t = t_0$ they can (at the expense of some effort) be matched smoothly to a surface within the dust cloud. If it can be shown that the resulting surfaces can be closed in the Friedmann part they will provide relevant information about the location of the boundary, and perhaps suffice to prove that the boundary $\mathcal{B}$ is spacelike where it joins the horizon. We think it would be interesting to carry such a calculation through.

We remark that it is easy to show—using a perturbation argument as in Ref. [9] based on the stability operator for MTSs [10]—that every round sphere on the dashed null cone shown in Fig. 3, except the one that lies on the event horizon, can be perturbed so that it partly extends into the interior of the cone while remaining trapped. However, such arguments do not suffice to show that the boundary is spacelike where it meets the horizon.

Another possible line of investigation would be to find past barriers for trapped surfaces, lying to the future of the constant Kodama-time hypersurface Σ [9]. In Sec. V we showed that the hypersurface σ forms such a barrier for axially symmetric trapped surfaces reaching the center. But for more general trapped surfaces there is a problem with this. A spherically symmetric spacelike hypersurface within the dust cloud is defined by

$$\eta = \eta(\chi).$$

Let the eigenvalues of its second fundamental form be denoted by $(\lambda_1, \lambda_2, \lambda_2)$, and its timelike unit normal by $\vec{n}$. A surface of revolution within such a hypersurface can be defined by

$$\theta = \theta(\chi).$$

Let us furthermore assume that this surface is minimal within the hypersurface (and that it intersects the matching hypersurface in a circle, where it should be continued into Schwarzschild). Then its null expansions are determined by the mean curvature vector $\vec{H}$ contracted into the normal vector. For a surface of this kind it can be shown that

$$2\theta_{\pm} = \vec{H}(n) = \lambda_1 + \lambda_2 - \frac{(\lambda_1 - \lambda_2)\theta'^2 \sin^2\chi}{1 - \eta'^2 + \theta'^2 \sin^2\chi}. \qquad (46)$$

Hypersurfaces whose equatorial cross sections are (locally) marginally trapped surfaces—such as σ—are singled out by the requirement $\lambda_1 + \lambda_2 = 0$, and they obey $\lambda_1 > \lambda_2$. But then we see that any surface of revolution which is minimal within such a hypersurface will be genuinely trapped whenever $\theta' \neq 0$. Of course we have not shown that such surfaces can be turned into closed trapped surfaces when extended into the Schwarzschild region, but it is already clear that the local argument that shows Σ to be a past barrier for all trapped surfaces [9] does not carry over to σ in any simple way.

Finally we want to raise a curious issue. It is known that no observer in a pure Schwarzschild black hole can observe a trapped surface in its entirety [20]. The same is presumably true for the Vaidya solution, but certainly it is not true in the OS model. Can one pinpoint exactly what it takes for a trapped surface to be visible? A first suggestion—that outermost stable MTSs can never be fully observed—fails because an observer falling along the central world line in the Oppenheimer-Snyder spacetime can observe some of the stable marginally trapped surfaces that form the Schwarzschild part of the event horizon; see Fig. 1. Observe, however, that this is not the case for the Vaidya solution as represented in Fig. 2. Even though at the moment we simply do not know the final answer, we conjecture that the difference arises due to the fact that the spherically symmetric marginally trapped tube A3H is timelike in the former case, while it is spacelike in the latter. Other possible Penrose diagrams in spherical symmetry (for instance Figs. 5 and 6 in Ref. [9]) seem to support this idea, even though a proper proof would probably require some effort.

VII. CONCLUSIONS

The question that underlies our investigation is, in a dynamical black hole, where is the boundary of the region containing trapped surfaces? As in a previous investigation of the Vaidya spacetime [14] we focused on a special kind of trapped surfaces designed to reach this boundary at the center of spacetime—although they would probably be overlooked in a numerical simulation tied to a specific foliation. There are two major improvements compared to the previous investigation:

(i) We have ensured that the surfaces are everywhere differentiable.
The conditions for this to be true across a matching hypersurface are given in the Appendix, and may be of independent interest.

(ii) We have made a serious effort to optimize the construction.
Although a proof escapes us, we believe we have reached the boundary of the trapped region at the center of the Oppenheimer-Snyder dust cloud. Because our construction is fully explicit a rigorous temporal upper bound on the location of the boundary is achieved.

Various open issues were discussed in Sec. VI. We find it puzzling, and indeed intriguing, that the very simple questions we ask are so difficult to answer.

ACKNOWLEDGMENTS

I. B. and E. J. thank Istvan Racz for encouragement. I. B. was supported by the Swedish Research Council under

Contract No. VR 621-2010-4060. J. M. M. S. is supported by Grants No. FIS2010-15492 (MICINN), No. GIU06/37 (UPV/EHU), No. P09-FQM-4496 (J. Andalucía—FEDER) and No. UFI 11/55 (UPV/EHU).

APPENDIX

In this appendix we consider the question of how to deal with surfaces in spacetimes (M, g) that are the result of a matching between two, previously given, known spacetimes (M^+, g^+) and (M^-, g^-) across a (timelike for definiteness) hypersurface $\mathcal{E}$.

As is often the case—and sometimes unavoidable—the explicit coordinates used to describe such matched spacetimes (M, g) consist of two different, unrelated sets: one corresponding to the $+$ manifold M^+, the other corresponding to M^-. Even though one cannot even ask the question of whether the metric components, say, are differentiable functions across $\mathcal{E}$ in such coordinates, this leads to no conceptual difficulties because there are theorems [21–23] ensuring that—provided the proper matching conditions hold—there exists another coordinate system on any neighborhood $U(p) \subset M$ of $p \in \mathcal{E}$ such that the metric components are actually C^1 functions in this new set. These coordinates are called admissible [21,24], and are usually not constructed explicitly. Actually, in most cases their expressions will be rather difficult—if not impossible—to get in terms of explicit functions.

All this is well understood. However, we want to consider surfaces (codimension-two submanifolds) that cross the matching hypersurface $\mathcal{E}$. How can one be sure that a given surface is actually differentiable, without undesired "corners" or "spikes," and such that extrinsic quantities—as for instance the expansions—do not have jumps? We are going to provide a simple method to deal with this question without any knowledge of the admissible coordinates. To this end, a very brief summary of the junction conditions is in order; see Ref. [25], Sec. 3.8 for a summary.

Let $(M^\pm, g^\pm)$ be two smooth spacetimes with respective metrics $g^\pm$. Assume that there are corresponding timelike hypersurfaces $\mathcal{E}^\pm \subset M^\pm$ which bound the regions $V^\pm \subset M^\pm$ on each $\pm$ side to be matched. These two hypersurfaces are to be identified in the final glued spacetime, so they must be diffeomorphic. The glued manifold is defined as the disjoint union of V^+ and V^- with diffeomorphically related points of $\mathcal{E}^+$ and $\mathcal{E}^-$ identified. The matching depends crucially on the particular diffeomorphism used to identify $\mathcal{E}^+$ with $\mathcal{E}^-$, and we assume that this has already been chosen and is given, so that the matching hypersurface is uniquely and well defined. Henceforth, this identified hypersurface will be denoted simply by $\mathcal{E}$. A necessary requirement to build a spacetime with at least a continuous metric is that the first fundamental forms $h^\pm$ of $\mathcal{E}$ calculated on both sides agree, because then there exists a unique C^1 atlas on M, which induces the C^∞ structures on $M^\pm$ and such that there is a metric extension g defined on the entire manifold that coincides with $g^\pm$ in the respective $V^\pm$ and is continuous [22,23].

In practice, one is given two spacetimes $(M^\pm, g^\pm)$ and thus two sets of local coordinates $\{x^\mu_\pm\}$ *with no relation whatsoever.* Hence, one has two parametric expressions $x^\mu_\pm = x^\mu_\pm(\xi^a)$ of $\mathcal{E}$, one for each embedding into each of $M^\pm$. Here $\{\xi^a\}$ are intrinsic local coordinates for $\mathcal{E}$, greek indices run from 0 to 3, while small latin indices run from 1 to 3. For each $\pm$ sign, the three vector fields $e^\mu_b = \partial x^\mu_\pm/\partial \xi^b$ are assumed to be linearly independent at any $p \in \mathcal{E}$ and are tangent to $\mathcal{E}$. The agreement of the two $(\pm)$ first fundamental forms amounts to the equalities on $\mathcal{E}$,

$$h^+_{ab} = h^-_{ab}, \qquad h^\pm_{ab} \equiv g^\pm_{\mu\nu}(x(\xi)) \frac{\partial x^\mu_\pm}{\partial \xi^a} \frac{\partial x^\nu_\pm}{\partial \xi^b}.$$

In other words, the tangent vector fields have equal scalar products on $\mathcal{E}$ from both sides. We denote by $n^\pm_\mu$ two unit normals to $\mathcal{E}$, one for each side. They are fixed up to a sign by the conditions

$$n^\pm_\mu \frac{\partial x^\mu_\pm}{\partial \xi^a} = 0, \qquad n^\pm_\mu n^{\pm\mu} = 1,$$

and one must choose n^-_μ pointing outwards from V^- and n^+_μ pointing towards V^+—or the other way around. The two bases on the tangent spaces

$$\left\{n^{+\mu}, \frac{\partial x^\mu_+}{\partial \xi^a}\right\} \quad \text{and} \quad \left\{n^{-\mu}, \frac{\partial x^\mu_-}{\partial \xi^a}\right\}$$

are then identified, so that one can drop the $\pm$. Observe, however, that this identification is usually only abstract, as in practice one still uses both bases—each on its own coordinate system—to do actual calculations.

The complete set of matching conditions is then obtained by requiring that the Riemann tensor components have no Dirac-delta-type terms [22,23], and this amounts to demanding that the second fundamental forms of $\mathcal{E}$, as computed from both $\pm$ sides, agree on $\mathcal{E}$ [21,26], that is to say,

$$K^+_{ab} = K^-_{ab},$$
$$K^\pm_{ab} = -n^\pm_\mu\left(\frac{\partial^2 x^\mu_\pm}{\partial \xi^a \partial \xi^b} + \Gamma^{\pm\mu}_{\alpha\beta}(x(\xi)) \frac{\partial x^\alpha_\pm}{\partial \xi^a} \frac{\partial x^\beta_\pm}{\partial \xi^b}\right).$$

We are now in a position to answer the question we asked. Assume, thus, that the above procedure has been performed and we have a properly matched spacetime (M, g) which, nevertheless, is presented to us with the two portions $V^\pm$ and the two metrics $g^\pm$ described in their original (and unrelated) $\pm$ coordinate systems. Imagine that we wish to describe an embedded surface S of sufficient differentiability in this spacetime so that, in particular, the null expansions on S are continuous. How to proceed?

Consider for a moment that we have built an admissible coordinate system $\{x^\mu\}$ around a point $p \in \mathcal{E}$. This means that the metric g is C^1 across $\mathcal{E}$ in these coordinates, and that g coincides with, i.e., is isometric to—g^+ on V^+, and g^- on V^-. The surface S would then be described in parametric form by

$$x^\mu = \Phi^\mu(\lambda^B),$$

where the functions Φ^μ are sufficiently differentiable (say, at least C^3) and λ^B are local intrinsic coordinates in S. Now, capital latin letters $A, B, \ldots = 2, 3$. This implies that the vector fields tangent to S

$$\frac{\partial \Phi^\mu}{\partial \lambda^B}$$

possess components that are C^2 functions of the λ^B, and the components of the first fundamental form of S

$$\gamma_{AB} = g_{\mu\nu}(\Phi(\lambda))\frac{\partial \Phi^\mu}{\partial \lambda^A}\frac{\partial \Phi^\nu}{\partial \lambda^B}$$

are therefore C^1 functions of the λ^B. With respect to the normal 1-forms, any normal N_μ to S is defined by the condition

$$N_\mu \frac{\partial \Phi^\mu}{\partial \lambda^B} = 0,$$

and therefore its components $N_\mu(\lambda^B)$ can be chosen to be C^2 as functions of the λ^B. In particular, this will be the case for the two independent null normal 1-forms. Observe, however, that the contravariant components N^μ will, in general, be just C^1 functions. Despite this, the components of the second fundamental form relative to any normal N_μ,

$$K_{AB}(N) = -N_\mu\left(\frac{\partial^2 \Phi^\mu}{\partial \lambda^A \partial \lambda^B} + \Gamma^\mu_{\alpha\beta}(\Phi(\lambda))\frac{\partial \Phi^\alpha}{\partial \lambda^A}\frac{\partial \Phi^\beta}{\partial \lambda^B}\right),$$

are continuous functions of the λ^B, because so are the Christoffel symbols as functions of the admissible x^μ. Finally, the normal connection 1-form s_A on S, also called the third fundamental form of S, has the components

$$s_A = -m_\mu\left(\frac{\partial u^\mu}{\partial \lambda^A} + \Gamma^\mu_{\alpha\beta}(\Phi(\lambda))\frac{\partial \Phi^\alpha}{\partial \lambda^A}u^\beta\right)$$

in terms of any orthonormal couple u_μ, m_μ of normal 1-forms,

$$-u_\mu u^\mu = m_\mu m^\mu = 1, \qquad u_\mu m^\mu = 0.$$

It follows that the two summands between brackets in the expression for s_A are continuous functions of the λ^B, and thus so are s_A.

The above has been deduced using an admissible coordinate system that we will not generally have at hand. Still, the conclusions reached—namely the differentiability of the first fundamental form and the continuity of the second and third fundamental forms as functions of the λ^B—are invariant and can be enforced without the use of the admissible coordinates. This follows because all these geometrical quantities have components that are expressed in terms of the intrinsic local coordinates λ^B on S so that, as long as we can provide expressions for these on both sides as such functions, their continuity or differentiability can be explicitly required.

This works as follows. In the practical situation we will have to describe the surface S as composed of a piece S^+ embedded in V^+, another piece S^- embedded in V^-, and such that both pieces intersect the matching hypersurface $\mathcal{E}$ at the same set,

$$S^+ \cap \mathcal{E} = S^- \cap \mathcal{E} \equiv S|_{\mathcal{E}}. \tag{A1}$$

The embeddings will each be described by corresponding parametric functions,

$$x^\mu_\pm = \Phi^\mu_\pm(\lambda^B),$$

so that, first of all, we need to find the explicit expressions that solve the indispensable condition (A1), that is to say, we need to find the solution to the two systems of equations

$$x^\mu_\pm(\xi^b) = \Phi^\mu_\pm(\lambda^B).$$

This solution exists, and actually agrees on both sides, if the surface S does meet the matching hypersurface $\mathcal{E}$ and $S|_{\mathcal{E}}$ is well defined. Let such a solution be described by the explicit functions and constraints

$$\xi^b = \xi^b(\lambda^B_0), \qquad \mathcal{F}_\Omega(\lambda^B) = 0. \tag{A2}$$

Here, λ^B_0 denote the values of λ^B at the intersection $S|_{\mathcal{E}}$, that is, the solutions to the constraint equations $\mathcal{F}_\Omega = 0$. These may depend on the matching hypersurface $\mathcal{E}$ and on the spacetimes $M^\pm$.

We can compute the first fundamental form of S on each of its two pieces $S^\pm$ as

$$\gamma^\pm_{AB} = g^\pm_{\mu\nu}(\Phi_\pm(\lambda))\frac{\partial \Phi^\mu_\pm}{\partial \lambda^A}\frac{\partial \Phi^\nu_\pm}{\partial \lambda^B}.$$

Then, the condition that γ_{AB} are differentiable implies that we must require on $S_{\mathcal{E}}$

$$\gamma^+_{AB}|_{S_{\mathcal{E}}} = \gamma^-_{AB}|_{S_{\mathcal{E}}}, \qquad \left.\frac{\partial \gamma^+_{AB}}{\partial \lambda^C}\right|_{S_{\mathcal{E}}} = \left.\frac{\partial \gamma^-_{AB}}{\partial \lambda^C}\right|_{S_{\mathcal{E}}}. \tag{A3}$$

Observe that taking the values of these components at $S_{\mathcal{E}}$ amounts to setting $\lambda^B = \lambda^B_0$.

In order to deal with the rest of the continuity conditions, we must first of all identify properly, on the set $S|_{\mathcal{E}}$, the normal 1-forms that are defined on both pieces $S^\pm$ of S. This can be done by computing, on each side, their scalar products with the identified bases on $\mathcal{E}$. We must thus require for any normal 1-form N_μ to S

$$\begin{aligned} N^+_\mu(\lambda_0)n^\mu_+(\xi(\lambda_0)) &= N^-_\mu(\lambda_0)n^\mu_-(\xi(\lambda_0)),\\ N^+_\mu(\lambda_0)\frac{\partial x^\mu_+}{\partial \xi^a}(\xi(\lambda_0)) &= N^-_\mu(\lambda_0)\frac{\partial x^\mu_-}{\partial \xi^a}(\xi(\lambda_0)). \end{aligned} \tag{A4}$$

Note that, given the normal 1-form on one side, these can be seen as equations determining the normal 1-form on the other side if the surface S is well defined. Once we have the normals properly identified, we can compute the second and third fundamental forms on both sides by using the corresponding $\pm$ objects; in other words,

$$K^{\pm}_{AB}(N) = -N^{\pm}_{\mu}\left(\frac{\partial^2 \Phi^{\mu}_{\pm}}{\partial\lambda^A\partial\lambda^B} + \Gamma^{\pm\mu}_{\alpha\beta}(\Phi_{\pm}(\lambda))\frac{\partial\Phi^{\alpha}_{\pm}}{\partial\lambda^A}\frac{\partial\Phi^{\beta}_{\pm}}{\partial\lambda^B}\right),$$
$$s^{\pm}_A = -m^{\pm}_{\mu}\left(\frac{\partial u^{\mu}_{\pm}}{\partial\lambda^A} + \Gamma^{\pm\mu}_{\alpha\beta}(\Phi_{\pm}(\lambda))\frac{\partial\Phi^{\alpha}_{\pm}}{\partial\lambda^A}u^{\beta}_{\pm}\right),$$

and then we must require, by letting $\lambda^B = \lambda^B_0$,

$$K^{+}_{AB}(N)|_{S_\varepsilon} = K^{-}_{AB}(N)|_{S_\varepsilon}, \qquad s^{+}_A|_{S_\varepsilon} = s^{-}_A|_{S_\varepsilon}. \tag{A5}$$

In summary, given the discussion above in admissible coordinates, the set of conditions that we must require on S are

(1) the existence of a solution (A2) that defines the set (A1) unambiguously,
(2) the proper identification of normal 1-forms on $S|_\varepsilon$ according to Eq. (A4),
(3) conditions [Eq. (A3)] to allow for the differentiability of the first fundamental form on $S|_\varepsilon$, and
(4) conditions [Eq. (A5)] to comply with the continuity of the second and third fundamental forms.

Clearly, these conditions are necessary to have a well-defined surface S without corners, with no jumps in the expansions, etc. They are actually sufficient too, because if the surface S had a corner, or if its null expansions had a jump, etc., then some of them would not hold.

As a final comment, we want to remark that the construction carried out in a previous paper [14] was not completely correct in this sense, because the advanced null coordinates used there are not admissible (the metric has jumps in some of their first derivatives) while the built trapped surface was given parametrically in terms of those coordinates. This can actually be noticed because the expansions had a jump across the matching hypersurface.[1] Nevertheless, the surface could easily be smoothed out and the construction would still work.

[1]Even though the matching hypersurface in Ref. [14] is null, a similar treatment as the one herein presented can be carried out along the lines of Refs. [22,23].

[1] *Black Holes: New Horizons*, edited by S. A. Hayward (World Scientific, Singapore, 2013).
[2] A. Ashtekar and B. Krishnan, Living Rev. Relativity **7**, 10 (2004).
[3] I. Booth, Can. J. Phys. **83**, 1073 (2005).
[4] R. Penrose, Phys. Rev. Lett. **14**, 57 (1965).
[5] T. W. Baumgarte and S. L. Shapiro, *Numerical Relativity: Solving Einstein's Equations on the Computer* (Cambridge University Press, Cambridge, England, 2010).
[6] D. M. Eardley, Phys. Rev. D **57**, 2299 (1998).
[7] I. Ben-Dov, Phys. Rev. D **75**, 064007 (2007).
[8] S. A. Hayward, Phys. Rev. D **49**, 6467 (1994).
[9] I. Bengtsson and J. M. M. Senovilla, Phys. Rev. D **83**, 044012 (2011).
[10] L. Andersson, M. Mars, and W. Simon, Adv. Theor. Math. Phys. **12**, 853 (2008).
[11] J. Plebański and A. Krasiński, *An Introduction to General Relativity and Cosmology* (Cambridge University Press, Cambridge, England, 2006).
[12] I. Booth, L. Brits, J. A. Gonzalez, and C. Van Den Broeck, Classical Quantum Gravity **23**, 413 (2006).
[13] C. Williams, Ann. H. Poincaré **9**, 1029 (2008).
[14] I. Bengtsson and J. M. M. Senovilla, Phys. Rev. D **79**, 024027 (2009).
[15] J. R. Oppenheimer and H. Snyder, Phys. Rev. **56**, 455 (1939).
[16] A. N. Staley, T. W. Baumgarte, J. D. Brown, B. Farris, and S. L. Shapiro, Classical Quantum Gravity **29**, 015003 (2012).
[17] E. Poisson, *A Relativist's Toolkit: The Mathematics of Black-Hole Mechanics* (Cambridge University Press, Cambridge, England, 2004).
[18] A. B. Nielsen, M. Jasiulek, B. Krishnan, and E. Schnetter, Phys. Rev. D **83**, 124022 (2011).
[19] J. M. M. Senovilla, Classical Quantum Gravity **19**, L113 (2002).
[20] R. W. Wald and V. Iyer, Phys. Rev. D **44**, R3719 (1991).
[21] W. Israel, Nuovo Cimento B **44**, 1 (1966); **48**, 463(E) (1967).
[22] C. J. S. Clarke and T. Dray, Classical Quantum Gravity **4**, 265 (1987).
[23] M. Mars and J. M. M. Senovilla, Classical Quantum Gravity **10**, 1865 (1993).
[24] A. Lichnerowicz, *Théories Relativistes de la Gravitation et de l'Electromagnétisme* (Masson, Paris, 1955).
[25] H. Stephani, D. Kramer, M. A. H. MacCallum, C. Hoenselaers, and E. Herlt, *Exact Solutions to Einstein's Field Equations* (Cambridge University Press, Cambridge, England, 2003), 2nd ed.
[26] G. Darmois, *Les équations de la gravitation einsteinienne*, Mémorial des Sciences Mathématiques, Fascicule 25 (Gauthier-Villars, Paris, 1927).